Weld metal cracking in cellulosic welds of X80 steel

Muralitharan Suppiah
University of Wollongong

WELD METAL CRACKING IN CELLULOSIC WELDS OF X80 STEEL

A thesis submitted in fulfilment of the requirements for the award of the degree of

Master of Engineering (Hons)

From

THE UNIVERSITY OF WOLLONGONG

by

MURALITHARAN SUPPIAH

Department of Materials Engineering

1999

ACKNOWLEDGEMENTS

Its my privilege to express my deep sense of gratitude to

- Professor Druce Dunne, in his capacity as a supervisor for his support, advice, encouragement and patience to see this thesis to completion.
- Dr. Nazmul Alam, supervisor for his valuable guidance to greater clarification of academic knowledge and for many useful discussion, help and consistent support throughout this degree.
- BHP Steel Works, Port Kembla, for cooperation in the experimental welding work.
- Mr. Greg Tilaman and Mr. Nick Mackey for their assistance in metallography and SEM laboratories.
- All the staff of Materials Engineering who in any manner, directly or indirectly, put a helping hand in completing this thesis.

..... Finally,

- My family and friends for their love, belief, support and encouragement which helped me complete this degree.

CONTENTS

ABSTRACT

The development of steel chemistries which result in highly weldable niobium - molybdenum micro-alloyed thin walled, high strength X80 grade is resulting in increasing consideration for use by Australian industry, particularly in offshore and pipeline applications. Despite the significant material cost saving through reduced thickness and increased strength, a limiting factor controlling widespread use of X80 is the susceptibility to weld metal cracking. The excellent weldability of this grade of line pipe steel has enhanced the potential for the use of high strength cellulosic consumables like E 9010 and E 8010 in root pass welding, but the risk of hydrogen assisted cold cracking (HACC) is also increased because of the high strength weld metal. To quantify the cracking susceptibility and to alloy guidance for field welding condition, the Welding Institute of Canada (WIC) restraint test was used in the present investigation. This thesis outlines the use of two grades (E 9010 and E 6010) and five different brands of commercial cellulosic consumable to assess conditions leading to hydrogen assisted cold cracking and solidification cracking in the diluted weld metal. The investigation also involved clarification of the relationship between microstructure, preheat temperature and hardness values for the various weld consumables and their effect on cracking susceptibility.

Tests were carried out using a standard restraint length of 25mm on 8.6mm strip preheated to various temperatures to determine the critical crack free temperature. For E9010 electrodes, a preheat of 40°C or more was found to be effective and For E6010

electrodes, a preheat of 30°C or more was effective in avoiding cold cracks in the weld metal. Most of the cracks found on welds preheated at room temperature were initiated by a defective weld feature such as undercut or lack of penetration. An attempt was made to correlate the hardness values and carbon equivalents (IIW) of weld metal to cracking. However, it was found that there was no significant effect of these variables on cracking over the range of welding conditions investigated.

The cracking morphology studies indicated that there are many ways in which the crack can propagate in the weld and HAZ. The modes of cracking observed were microvoid coalescence, quasi cleavage and intergranular. In some cases solidification cracking was detected.

The testing program indicated that despite the high hydrogen content of the weld metal for E 9010 electrodes, crack-free root pass welds can be obtained for 8.6mm X80 steel strip provided a preheat of 40°C or higher is used to ensure a low cooling rate.

INTRODUCTION

The Australian gas pipeline industry started significant projects in the 1960's and there has been a significant upsurge in construction since then. The development of pipeline steel is a continuous improvement process driven by complex interaction of many factors. Over the recent years, some 90,000 tonnes of X70 grade has been successfully applied to several Australian projects. The importance of achieving high strength in pipes without compromising field weldability has been a major focus in the evolutionary development of X70 grade, which has effectively laid the foundation for X80 grade pipeline. X80 pipeline steel provides good potential for reliable low cost construction of oil and gas pipelines, decreased transport to site cost, reduced welding cost due to smaller and thinner wall thickness. The improved alloy design for X 80 grade using the carbon, manganese, niobium, molybdenum and titanium (C - Mn - Nb -Mo - Ti) system is based on a low carbon content, a restricted IIW carbon equivalent (CE_{IIW})*, niobium addition for grain size control and precipitation hardening and titanium to restrict grain growth during rolling and the weld thermal cycle. Molybdenum (Mo) is used to increase the hardenability and increase the strength through the formation of fine low carbon bainite. The use of cellulosic electrodes in pipeline welding offers high arc stability and good root penetration at high travel speed. However, the electrodes must also produce strength matching weld metal which is crack free.

---

* $CE_{IIW} = C + Mn/6 + (Cr + Mo + V)/5 + (Ni + Cu)/15$

The Welding Institute of Canada (WIC) restraint test was adopted to carry out the laboratory welding, because it was considered that field welding stress conditions can be closely simulated using this test. Two grades of commercial (E 9010 and E 6010) consumables were investigated with standard restraint lengths of 25mm and different preheat temperatures. The critical preheat temperature to avoid hydrogen assisted cold cracking (HACC) in the weld metal was determined.

Microscopic studies of the samples were carried out using optical microscopy. Hardness tests were conducted on HACC and solidification cracked samples. An attempt was made to relate microstructure and fracture topography. Finally scanning electron microscope studies were carried out to study the nature of HACC and solidification cracked fracture surfaces.

Chapter One

1.0 OVERVIEW OF HIGH STRENGTH LINEPIPE

Tubes and pipes have become important engineering structures in the energy industry since the world war. Exploitation of oil and gas fields has driven the use of these engineering structures to transport fluids over long distances. Technological advancement in steel making has offered the opportunity to apply different grades of pipe steel particularly X70 and X80 steels over the last decade. The replacement of older thick walled, large diameter pipeline with high strength thin wall pipeline has given researchers a challenge to optimise all production steps from steel making through to pipe laying. The economic benefits of high strength pipelines such as reduced gas transportation costs, high gas pressure and flow rates, lower pipe procurement, lower transport-to-site cost, reduced welding cost due to smaller diameter and thinner walls has favoured their use in Australia [1, 2].

1.1 CHARACTERISTICS OF HIGH STRENGTH PIPELINES

The rapid progression towards the use of high strength thin wall pipeline over the past decade has seen the pipe grade move from API 5L X52 through to API 5L X80 with maximum operation pressure rising from 6.8 MPa to 15.3 MPa. The increasing use of high strength ERW linepipes over the years has been shown in Figure 1.1 [2].

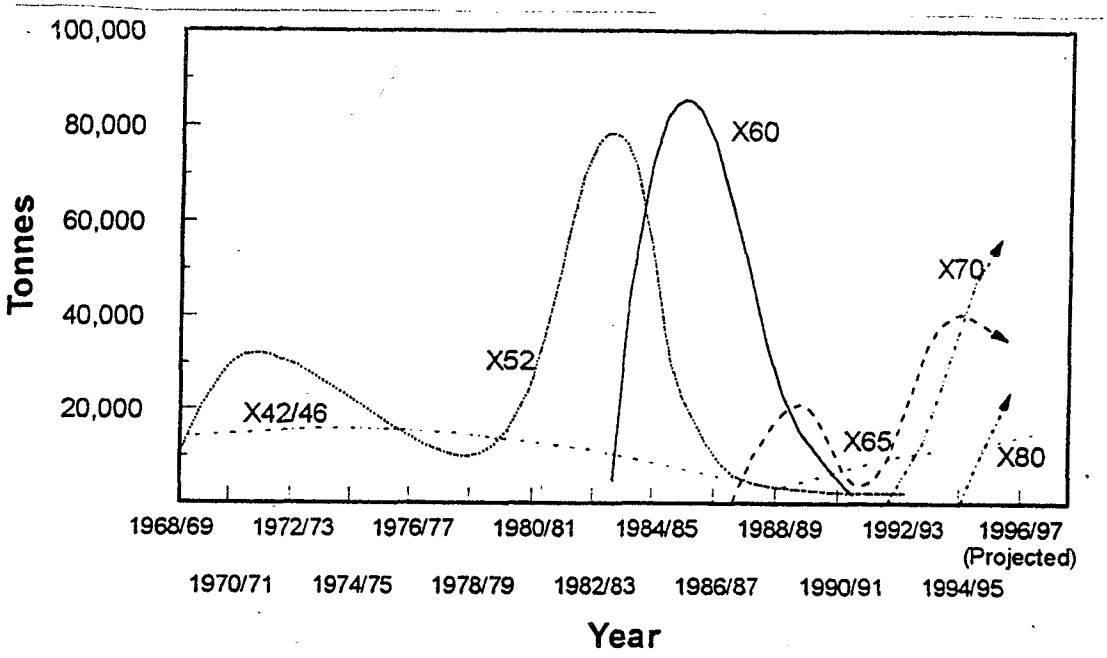

Figure 1.1 : ***Usage of higher strength ERW linepipe in Australia [2].***

The grade X80 has not been applied to any significant ERW pipeline in the world but has high potential for its application in future Australian projects [1]. Special issues concerning the application of X80 grade are selection of consumable, preheat free welding with cellulosic electrodes and requirement for high toughness as reflected in high Charpy energy values. This last issue is important in rich gas transportation. The introduction of X80 grade pipe has raised two important issues for the use of cellulosic consumables:

1. adequate weld to parent /pipe metal strength matching; and
2. weldability particularly in terms of hydrogen assisted cold cracking in weld metal and heat affected zone (HAZ)

1.2 CHEMICAL COMPOSITION AND ALLOY DESIGN

The chemical compositions of pipe steel manufactured in Australia over recent years are shown are Figure 1.2

Steel	API Grade	Chemical Composition, Mass %												CEQ (IIW)	Pcm
		C	Mn	Si	P	S	Al	Nb	V	Mo	Ti	N	Ca		
ERW Pipe from Full Width Strip															
A	X60	0.080	1.25	0.12	0.017	0.003	0.025	0.040	-	-	0.013	0.0050	0.0025	0.29	0.15
B	X65	0.080	1.45	0.12	0.017	0.003	0.025	0.038	0.042	-	0.012	0.0050	0.0025	0.34	0.16
C	X70	0.085	1.50	0.32	0.015	0.001	0.030	0.045	0.050	-	0.013	0.0045	0.0008	0.36	0.18
D	X70	0.095	1.55	0.32	0.015	0.001	0.030	0.040	0.060	-	0.013	0.0045	-	0.37	0.19
E	X70	0.060	1.35	0.32	0.013	0.003	0.030	0.060	-	0.23	0.014	0.0050	0.0008	0.34	0.16
F	X70	0.070	1.50	0.32	0.012	0.005	0.030	0.060	-	0.11	0.015	0.0050	0.0008	0.34	0.17
G	X80	0.075	1.59	0.31	0.018	0.001	0.026	0.057	-	0.22	0.013	0.0060	0.0011	0.38	0.18

Figure 1.2 : ***Typical chemical compositions of ERW high strength line pipe steels [1]***

In higher strength steels, emphasis is placed on low carbon and reduced manganese content to reduce levels of centerline segregation [1]. High peak segregation levels on the strip centre line in association with excessive fibre upturn in the process and non-optimum cooling condition following seam annealing could compromise weld ductility. Low C - Mn alloy design concept is applied which is similar to hydrogen induced cracking (HIC) resistant line pipe steels. HIC susceptibility is increased by the hard phase centerline segregation microstructures.

Calcium is used for globular complexing of alumina inclusions and micro titanium additions which reduces the susceptibility of cold cracking in the HAZ. The other important alloy design principles involve niobium (Nb) and vanadium (V) for ferrite grain refinement, precipitation hardening and silicon (Si) for compensatory strengthening. The addition of molybdenum (Mo) increases the volume fraction of acicular ferrite and M-A with increased grain refinement and precipitation hardening. Essentially the use of Mo has allowed low carbon equivalents and permitted safe field welding with cellulosic electrodes in the higher strength X70 and X80 grades of line pipe [1,3]

1.3 PRODUCTION PROCESS FOR STEEL

The steel making units involved in the production of line pipe steel are schematically shown in Figure 1.3

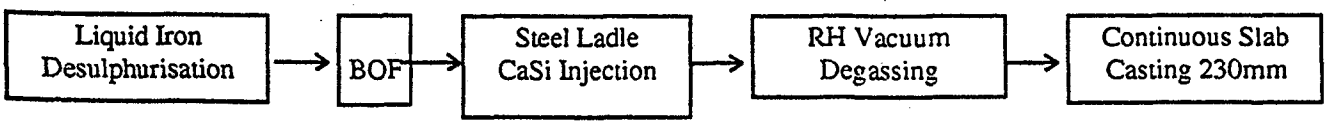

Figure 1.3: ***Compositional control of steel [1].***

Desulphurisation treatment and subsequent slag raking of liquid iron achieve low sulphur contents. This improves the fracture toughness requirements to avoid ductile fracture propagation in X60 to X80 grades of pipe. Much lower sulfur content from 0.005% to 0.003% results in the higher Charpy energy values which are required to ensure ductile fracture resistance for rich gas transportation. To avoid effects of clustered alumina inclusions on the weld zone, an appropriate amount of calcium is added to form low melting point $(CaO)_{12}$ $(Al_2O_3)_7$ inclusions which can be obtained by lime/fluorspar addition followed by argon bubbling and calcium silicate (CaSi) ladle injection. Vacuum degassing treatment enhances chemical control of specified microalloy elements. Vacuum degassing after CaSi injection facilitates floating of calcium aluminates without the risk of oxidation or nitrogen pickup and achieves lower volume fractions of globular inclusions.

1.3.1 Control of centerline segregation

As said earlier, C and Mn contents have a major influence on centreline segregation levels in continuously cast steels. To minimise both volume fraction of hard phase centreline microstructures and low segregation ratio of hardenability enhancing elements such as Mn in the segregation bands, various casting countermeasures together with low C - Mn alloy design are used. Microprobe measurements of Mn concentration in second phase bands across the centreline region of both conventional high Mn and lower C - Mn alloy designs clearly reveal peak Mn levels well below 2.0% as shown in Figure 1.3.1. Such levels of Mn together with low carbon contents

considerably reduce the potential for martensite formation in the hot rolled and strip and plate.

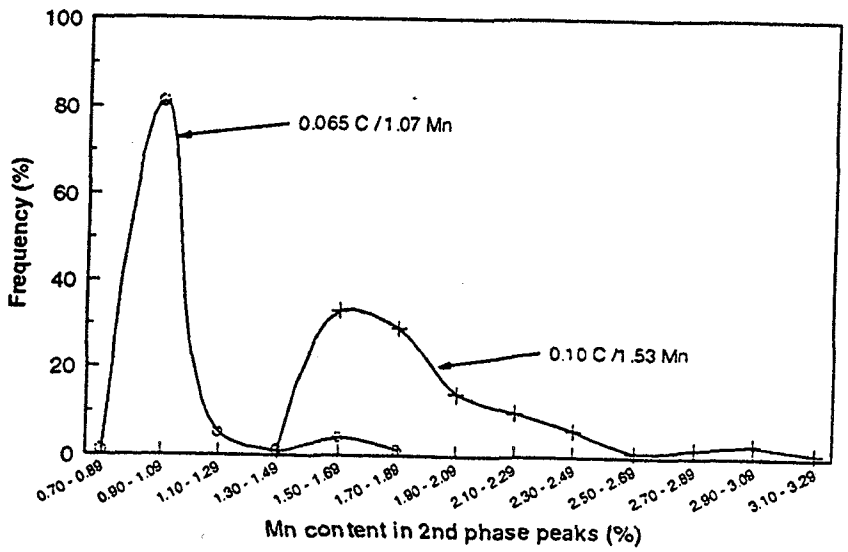

Figure 1.3.1: ***Microprobe analysis of Mn across centreline region in high and low C- Mn line pipe steels [1].***

1.3.2. Hot Strip Rolling

Proper control of the entire rolling process from slab reheating to coiling is essential to develop the appropriate strength and fracture toughness requirements to permit trouble free field welding with cellulosic electrodes. Some important considerations in the hot strip rolling are mentioned below.

(1) **Slab Reheating**: The main aim is to achieve uniformly heated slabs with complete solution of the microalloy carbonitrides. The slab reheating temperature is 1250^0 C. The uniform reheating concept provides uniform mechanical properties

within the coils but also from coil to coil. This is also a prerequisite for tight thickness control for pipe manufacturing.

(2) **Rough rolling or coil box**: The rough rolling phase is completed at temperatures above about 1030^0 C with the metallurgical objective of achieving the finest possible recrystallised austenite grain size and TiN particle control to inhibit growth of recrystallised grains. The transfer bar thickness is about 26 - 30mm for linepipe coils in the thickness range 70 - 80%.

(3) **Finish rolling**: This stage is generally commenced below the austenite recrystallising temperature (about 950^0 C for Nb and Nb/V steels and about 1000^0 C for Mo-Nb steels). The main intention of this phase is to achieve a high rolling strain within the austenite grains so that a very fine ferrite grain size can be generated during controlled cooling in the hot strip mill.

(4) **Run out table cooling/ coiling**: The coiling temperature and cooling pattern are vital in achieving optimum strength by controlling the influence of transformation microstructures, ferrite grain refinement and precipitation hardening. In Mo - Nb steels, such as X80 high cooling rates immediately after finish rolling can result in a fine acicular ferrite structure with increased strength and toughness.

1.4 PIPE STEEL PROPERTIES AND PROCESSING

The most critical aspects of pipe making from the mechanical perspective are cold forming and sizing which affect the pipe yield strength. When hot rolled strip is converted to ERW pipe, material and processing factors contribute in a complex

manner to the strength change by the virtue of Bauschinger effect and work hardening behaviour. The loss of strength increases generally with increasing strip strength, requiring allowance to be made in the design of higher strength steel grades such as X70 and X80.

The major consideration in the design of X80 grades of linepipes has led to achieving higher strengths comfortably by means of adding molybdenum, whilst avoiding the excessive use of high carbon equivalent (CE). The additions of Mo in niobium (Nb) steels provide compensatory strengthening over conventional (V - Nb) steels. The main factors contributing to this effect are as follows.

A finer (often irregularly shaped) ferrite grain size. These grains are characterised by an extensive network of subgrains.

Replacement of pearlite by low transformation products, mainly bainite containing acicular carbide needles.

Enhanced precipitation hardening from the Mo - Nb system.

1.5 WELDABILITY

Weldability is defined as ' the capacity of a material to be welded under the imposed fabrication condition into a specific, suitably designed structure and to perform satisfactorily in intended service ' [5]

In the past decade, the shift towards the use of higher strength thin walled pipeline grades has imposed severe demands on pipe steel properties and welding technology to ensure high quality, safe and economic installation and operation. Technological advancements in steel making particularly titanium treatment has increased the resistance to heat affected zone (HAZ) cracking, which has been a ongoing defect faced by the researcher and pipeline industry over past decades [1, 4, 5].

Recent weldability studies [1, 2 ,3 , 5] show, the Nb - Mo steels exhibit excellent weldability compared to the conventional Nb - V steels. Experience with heavier wall thickness pipes in Europe and North America, suggest that high strength thick wall pipe should not be welded throughout with cellulosic electrode which is the most common and popular welding method that is being used to join pipelines. The Australian oil and gas pipeline industry serves relatively small markets generally at great distances from the source and as a consequence, design procedures are generally for small diameter and thin walled pipelines. The challenge for the Australian pipeline industry is to investigate the potential avenues to ensure weld integrity of these high strength Mo - Nb pipeline steels with currently available welding consumables.

Increased attention has been given to matching weld and pipe strengths by increasing the alloying elements in the consumable ie. by increasing the carbon equivalent (CE_{IIW}). Increased CE, at any cooling rate can increase susceptibility to cracking. However, the benefit of using thin wall pipe is to reduce the cooling rate and thereby

reduce the development of susceptible microstructures. Field weldability studies carried out on X80 grade show excellent results can be achieved with cellulosic consumables compared with X70 grade[2, 3]. This provides confidence to the pipeline industry for the potential to install and safely operate thin walled high strength pipes for future pipeline projects, but more detailed laboratory investigations, such as the one conducted in this investigation, are necessary to define boundary conditions to avoid cracking.

Chapter Two

2.0 WELDING PROCESS AND CONSUMABLES

Despite the trend towards automation, the on shore construction / laying of transmission pipelines is still predominantly carried out by using the Manual Metal Arc Welding (MMAW) process. It is still the dominant joining method in Australia since its inception in the 1920s [5]. Among the number of reasons for the trend, the most often quoted fact is the resistance of this process to adverse weather conditions and thus even in unfavourable terrain, laying of pipelines can be carried out cost effectively.

2.1 MANUAL METAL ARC WELDING PROCESS (MMAW)

Manual Metal Arc Welding is one of the most common of the fusion welding processes. The heat source is provided by an electric arc, a high current and a low voltage discharge in the range of 10 – 500 A and 10 – 50 V. The consumable / electrode consists of a core wire of filler wire and a flux coating composed of various silicates and metal oxides. During welding the flux decomposes to form a viscous slag which provides a protective layer between the atmosphere and the molten metal. Figure 2.1 illustrates the MMAW process.

In addition, the slag creates a chemically reducing environment, which helps to exclude elements in the air and to prevent moisture from penetrating the weld pool. It also generates gases, which help maintain the flow of liquid metal droplets from the

filler wire to the pool. The slag adequately covers the melt, even in vertical welds, and so its composition is critical as this affects the viscosity. The slag is also easily detachable from the solidified weld surface [5].

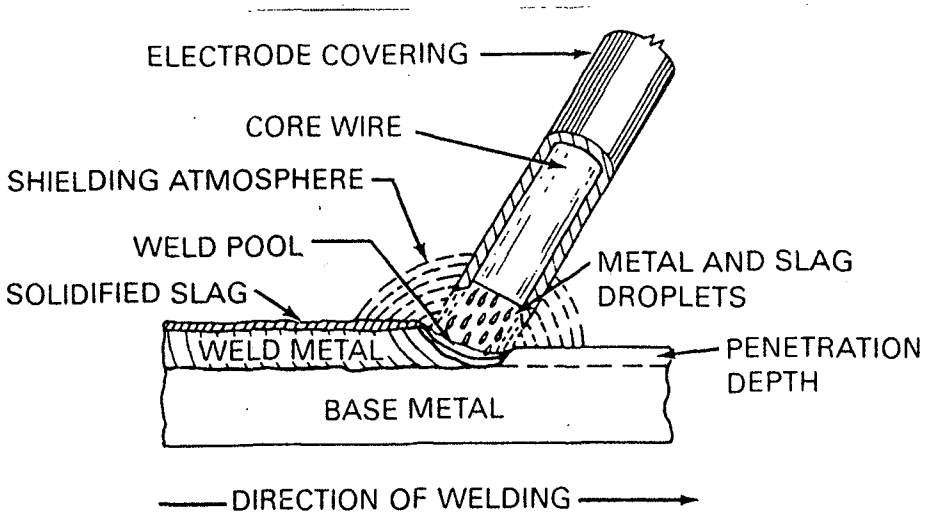

Figure 2.1: ***Manual Metal Arc Welding Process [5].***

Although, it is the dominant joining process in the pipeline industry, MMAW has both advantages and limitations. The process has versatility, mobility, cost effectiveness and results in the metallurgical requirements which are essential in pipe laying / construction. However, limitations are difficulties with high hydrogen weld metal, non continuous welding and requirement a for high operator / welder skill.

These limitations can compromise the weld integrity and performance of the line pipes.

2.2 CONSUMABLES

Consumables for SMAW have many different compositions for the core wire and a variety of types and weights of flux covering to suit the application. The flux composition strongly determines the quality and soundness of the weld metal. The two principal type of consumables employed in joining pipe are:

(1) Cellulosic Electrode

(2) Basic Electrode

The classification of low carbon steel electrode according to the AWS, is generally followed throughout the industry. In this system an electrode is represented by the code,

EXXXX

E : represents the electrode

XX : the first to two digits indicate tenths of minimum tensile strength in MPa of deposited weld metal in as welded conditions. For eg: E9010 has minimum tensile strength of 620 MPa

X : the third digit indicates the welding position

X : finally the fourth digit represent the type of covering. The following table shows the electrode covering.

Fourth digit	Covering	Current(a)
0	High cellulose, sodium(b)	DCEP(b)
	High iron oxide(c)	ac or dc(c)(d)
1	High cellulose, potassium	ac or DCEP
2	High titania, sodium(e)	ac or dc(f)
3	High titania, potassium	ac or dc(f)
4	Iron powder, titania	ac or dc(f)
5	Low hydrogen, sodium	DCEP
6	Low hydrogen, potassium	ac or DCEP
7	Iron powder, iron oxide	ac or dc(d)
8	Iron powder, low hydrogen	ac or DCEP

Table 2.2: *Different electrode covering according to AWS classification [5].*

2.2.1 Cellulosic Electrodes

Commercial cellulosic electrodes are widely used for high productivity welding in the Australian pipeline construction industry. These electrodes contain cellulose (30 – 40%), silicates (slag formers) and rutile (arc stabilisers) which release copious quantities of gaseous hydrogen and carbon mono-oxide around the arc during

operation [9, 10]. The presence of high hydrogen content helps stabilise the arc and creates conditions in the arc atmosphere which promote flow of molten metal improving the root penetration where access is only possible from one side [9].

In practice, the laying speed of pipeline construction is influenced by the degree of planning and overall welding sequence. The use of cellulosic consumables for the root pass by allowing high welding speeds (despite its high hydrogen concentration) has an advantage in reducing the cost. The Figure 2.2.1. shows welding speeds of two different electrodes principally used in welding pipelines.

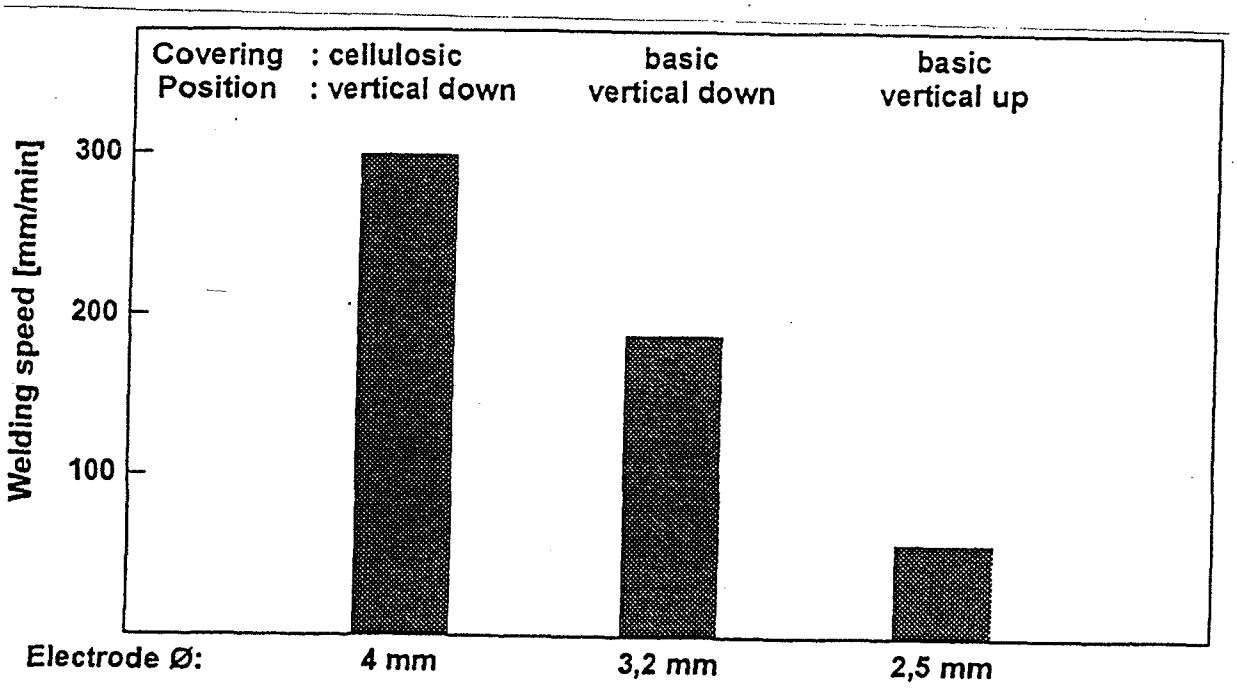

Figure 2.2.1: ***Welding speed in root pass welding with different types of electrodes [11].***

It can be seen that cellulosics electrode have an advantage over basic electrodes in speed at which the root pass is completed (300mm/min compared to 190mm/min). However, it should be noted that the basic electrodes referred in Figure 2.2.1 are 3.2 and 2.5mm in diameter which will require lower currents and produce smaller deposition rates than the 4mm cellulosic electrodes. Thus the advantages of cellulosic electrodes indicated in Figure 2.2.1 are probably exaggerated.

A comparative root welding study by Bruche and Muesch [11], on X80 thin wall pipe with cellulosic and basic electrodes shows increased welding speeds are achieved using cellulose and basic electrode combinations as shown in Figure 2.2.2.

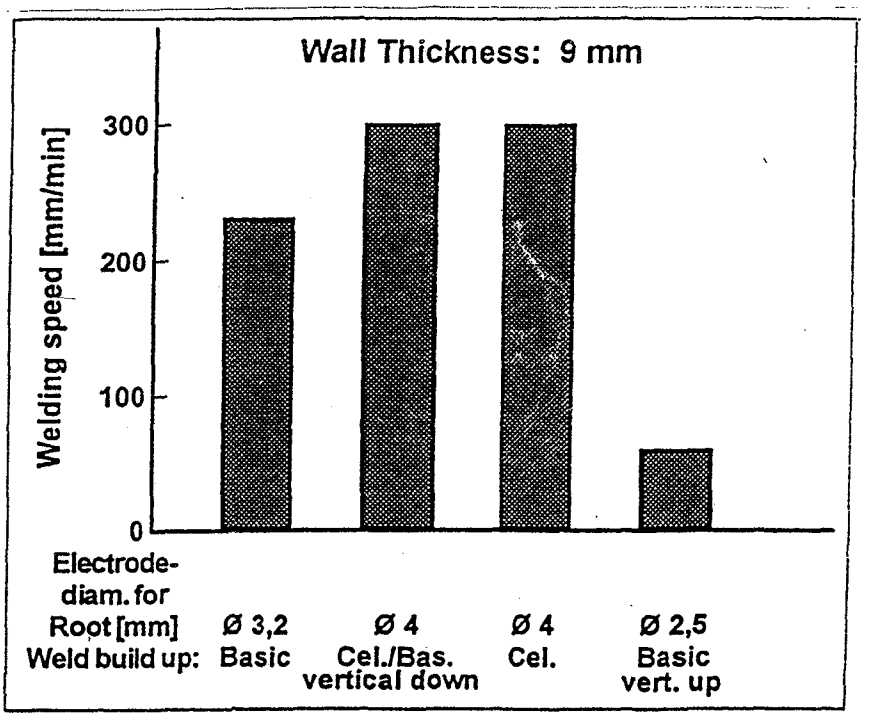

Figure 2.2.2: ***Welding speed in root pass welding with different types of electrodes on 9mm thick X80 grade pipe [11].***

There are many factors that contribute to the overall strength and soundness of the weld metal. The use of strength matching cellulosic consumable and their properties are discussed in the following chapters. Major concerns have been expressed that electrode performance can significantly vary from manufacturer to manufacturer and in the worst case from batch to batch. Such variation is an impediment to the development of weldments of acceptable structural integrity and reliability [10]. Although, as reported in the previous chapter, the weldability of high strength X80 pipe grade is high [1, 2, 10], but there is concern about achievement of good weldability and the cracking resistance of strength matching cellulosic electrodes.

Chapter Three

3.0 HOT AND COLD CRACKING IN HIGH STRENGTH STEELS

Hydrogen assisted cold cracking has been an important topic for many years particularly in the on and off shore pipeline construction industry. Extensive research studies have been undertaken to quantitatively analyse the problem. In conventional carbon - manganese (C - Mn) structural steels the presence of hydrogen has been proved to be very critical due to relatively high carbon contents. Hydrogen assisted cold cracking (HACC) was mainly confined to the heat affected zone (HAZ) of the weldment [5, 13, 14, 16, 17, 20, 21]. Recent developments in modern structural steels with low carbon content and improved alloy design has shifted the potential cold cracking to the weld metal [5, 12, 13, 14, 28]. There are many factors that contribute to the HACC in the weldment. They are

(1) weld metal hydrogen

(2) stress concentration (high tensile stresses)

(3) susceptible microstructure

Hot cracking is currently is not as significant a problem as cold cracking and the conditions leading to hot cracking are generally well known and it can be avoided by control of the welding conditions.

3.1 HYDROGEN ASSISTED COLD CRACKING

Hydrogen is a ubiquitous contaminant in all arc welding processes. It exists in fluxes, organic lubricant on surface of the filler wires, debris that collects in the weld joints, moisture in the air and cellulosic electrodes that can be aspirated into the arc stream [5, 8]. Hydrogen has a much higher solubility in molten iron (liquid state) than in solid iron. Its solubility decreases with temperature in the solid state. The hydrogen solubility in iron as a function of temperature is shown in Figure 3.1.1

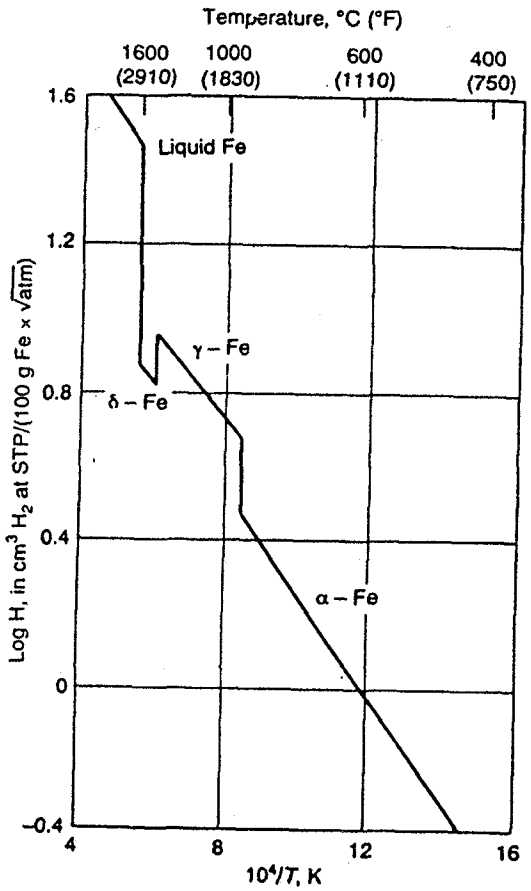

Figure 3.1.1 : ***Effect of temperature on the solubility of hydrogen in Iron [5].***

In the liquid state (1500°C) the solubility of hydrogen is about 30ppm by weight but it drops to 1ppm at 400°C (solid state - α iron). The weld metal solidifies at a high rate and hydrogen that has dissolved in fused weld metal is retained in the solid state. Although it does escape as gas, it is often trapped in the form of gas bubbles (weld metal porosity). But a substantial amount remains in the solidified weldment as **'supersaturated hydrogen'**. It should be understood that as little as 1ppm of hydrogen in the weld metal can cause cracking problems in high strength steels [5, 6, 7, 21, 28]

3.1.1 Measurement of Hydrogen

Direct measurements of hydrogen in weld metal are very difficult in practice, however, and the test procedures recommended by AWS to measure the volume of hydrogen gas escaping from the weld metal for different welding processes are as follows. Hydrogen gas is collected either in a eudiometer tube (mercury / glycerine bath) or the isolation chamber of gas chromatograph.

ELECTRODE TYPE	**DIFFUSIBLE H2, ml/ 100g**
GMAW SOLID WIRE	0 - 10
SMAW BASIC ELECTRODE	3 - 20
SMAW ACID ELECTRODE	20 - 40
GMAW CORED WIRE	3 - 30
SAW SOLID WIRE AND FLUX	4 - 20

Table 3.1.1: ***Effect of welding processes and electrodes on hydrogen levels in welds [5].***

From Table 3.1.1 it is evident that the welding processes that use flux or flux covered consumables tend to produce increased diffusible hydrogen contents. The rate of moisture pick up depends on the constituents in the coating. Rebaking the electrodes can limit the amount of absorbed moisture from the atmosphere [5, 6].

3.2 STRESSES

Stresses play a major role in cracking phenomenon in high strength steel weldments. Stresses can occur both internally and externally. When weld metal solidifies the atomic hydrogen diffuses rapidly into the weld HAZ, some escaping and the rest remaining in the weld metal. These highly mobile atoms are trapped at discontinuities in the metal lattice and concentrate at those points. External restraint and volume changes can enlarge the discontinuity to form microcracks. The high stress concentration is relieved as the crack propagates. Cracking can be arrested if hydrogen escapes in a sufficient amount to lower its concentration below that which is needed for cracking to proceed. For example, underbead cracks can reduce the residual stresses in the weld below the needed level for propagation.

HACC does not always occur spontaneously. Weld metal hydrogen cracking can often be delayed by weeks or months as with heat affected zone cracking observed in conventional C - Mn steels. Inspection procedures must recognise this delayed occurrence [5, 12, 13, 21, 29]. Figure 3.2.1 illustrates the sensitivity of HACC to the level of external stress [17].

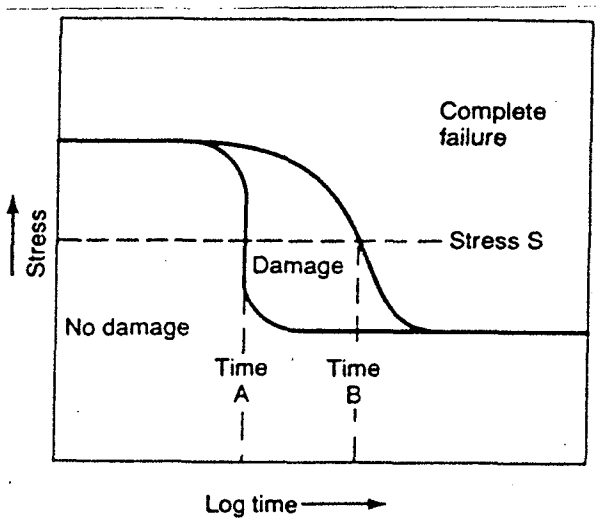

Figure 3.2.1 : ***Damage caused by HACC as affected by applied stress [5].***

It is believed that [5, 12, 16, 17] failure occurs in a structure when the stress exceeds the tensile strength of the specimen. However, with sufficient hydrogen, a stress well below the tensile strength also can initiate HACC. The most important observation is that HACC does not occur below a critical stress. High hydrogen content and low stress or vice versa can increase or reduce the time for initiation of the crack. The interaction between these two variables is shown in Figure 3.2.2. The time to initiate the hydrogen cracking and critical stress below which failure will not occur are inversely proportional to the amount of hydrogen present in the structure.

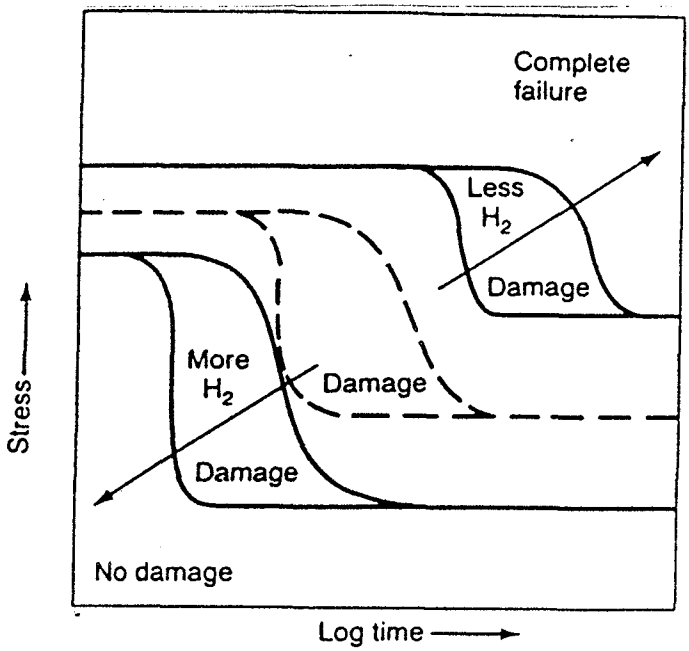

Figure 3.2.2 : ***Effect of hydrogen and stress on damage caused by HACC [5].***

3.3 SUSCEPTIBLE MICROSTRUCTURE

The third variable that affects HACC is microstructure. It has been found that steels containing higher carbon content as in C - Mn steels are more prone to HACC due to the formation of twinned martensite type of microstructure [5, 6, 7, 22, 25]. The technological advancement in steel production has resulted in making newer higher strength low carbon steel whose acicular ferrite microstructures provide more resistance to HACC.

The Figure 3.3.1 illustrates steel with relatively tolerant microstructure can exhibit a higher critical stress than a stronger steel with a sensitive microstructure. Stronger steels are more sensitive to hydrogen with regard to both an earlier initiation for HACC and lower critical stress [5, 7].

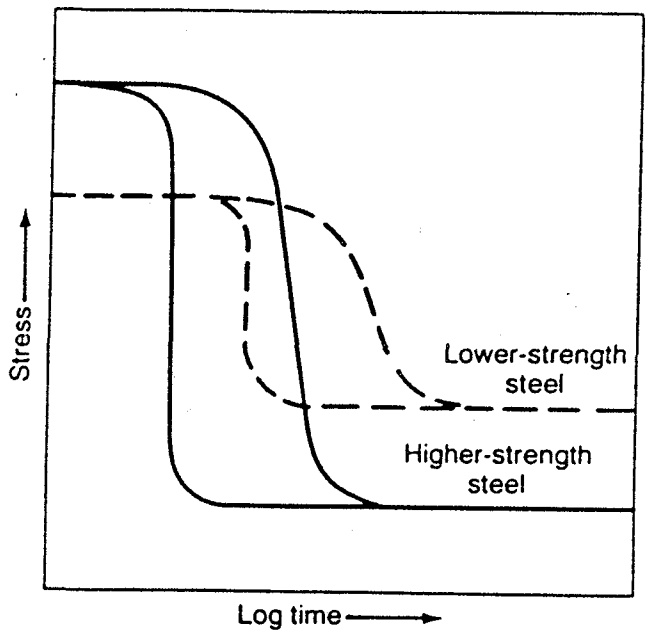

Figure 3.3.1 : ***Effect of steel strength on susceptibility to HIC damage [5].***

3.4 CRACKING MORPHOLOGY

Weld metal cracking may occur either transverse or longitudinal to the weld direction depending on the gaps, notches and the direction of the controlling stresses. In root runs of multipass welds, the root pass provides a stress concentration with respect to

stresses transverse to the weld leading to longitudinal cracks, which are a predominant form of cracking in pipelines [15, 16, 21]. Usually in multipass welds, cracks tend to propagate though ferrite veins from the fusion boundary at an angle of 45 . to the direction of tensile force showing a zig zag pattern of cracking called chevron cracking [3, 5, 16, 26].

Weld metal cracking is often associated with high a degree of plastic strain and cracks reveal wide and narrow section linkages. The commonly observed feature of such cracks is occurrence along grain boundary ferrite located at prior austenite and solidification cell boundaries. According to the Beachem theory [15, 16] HACC fracture surfaces in the weld metal can form microvoid coalescence (MVC) intergranular fracture (IG) and quasi cleavage (QC). The theory also postulates that hydrogen promotes every fracture mode that is allowed by the local microstructure. The theory also shows that with decreasing stress intensity cracking propagates by processes which involve less plastic deformation, QC and IG. A SEM study by Matsuda showed cracking occurs in isolated locations and links up with existing cracks which takes place along slip bands across martensite laths with a QC fracture surface [15, 16, 29]. Figure 3.4 shows typical crack initiation and propagation, with the broken line indicating the intense plastic strain region, and the link segments which occur by QC.

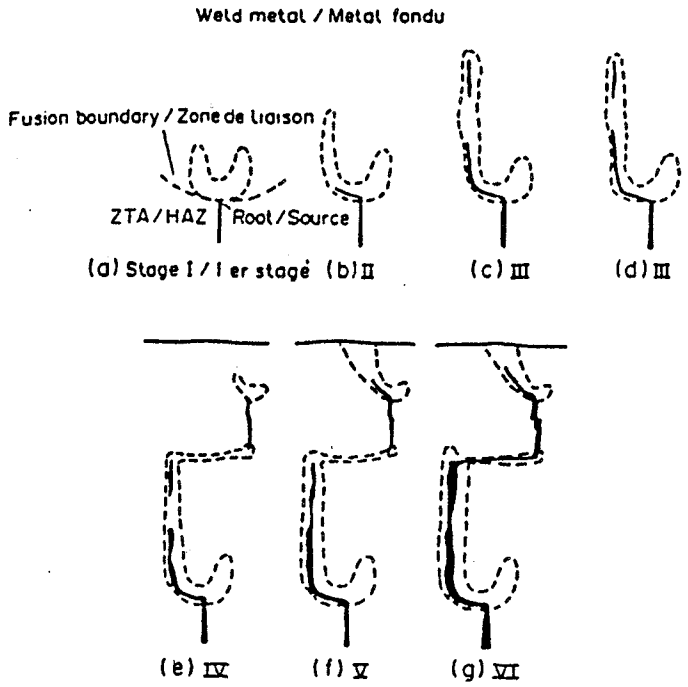

Figure 3.4 : ***Microscopic mode of crack initiation and propagation [16].***

3.5 CONTROL OF HYDROGEN ASSISTED COLD CRACKING

It is evident from the studies carried out by researchers that the three major factors influencing cold cracking must be present simultaneously [5, 6, 7, 13]. The approaches taken to prevent its occurrence are as follows:

(1) reducing stresses associated with the weldment eg. defect free welds;

(2) preheating prior to welding - to reduce the cooling time especially for $\Delta t_{8/1}$, where microstructures is important and time is required for hydrogen molecules to escape from the weldment;

(3) selecting a proper consumable and process for the application; and

(4) choosing the right design, joint configuration and skilled operators for the job.

In most cases compromises have to be made and a combination of these approaches probably will prove to be more cost effective.

3.6 HOT CRACKING

Hot cracking is usually regarded as a synonymous term for solidification cracking; but hot cracking can also occur in the solid state due to low hot ductility. Solidification cracks are in general well understood, unlike hydrogen assisted cold cracking. The partitioning and rejection of alloying elements at columnar grain boundaries and ahead of the advancing solid - liquid interface causes a marked segregation due to shrinkage strains resulting in cracks in the weld centre. The cracking that occurs between the columnar grains is called 'dovetail' cracking because of the shape of the weld associated with these cracks. The susceptibility of weld metal to this type of cracking depends on three main factors [5].

(1) The coarseness of the solidification microstructures

(2) The amount and type of segregated species

(3) The geometry of the joint and weld pool

3.6.1 Solidification Structures

Epitaxial solidification causes coarseness of the weld deposit microstructures to be inherited from the grain growth zone of the heat affected zone (HAZ). High energy welds have the largest grain growth and hence the coarsest microstructures in the weld. Welding speed plays a vital role in the solidification pattern, which determines the depth to width ratio. Low speeds allow columnar grains to follow the arc, curving in behind the moving heat source, and allowing grain refinement through nucleation of new grains along the < 100 > directions.

On the other hand, high travel speed tends to produce columnar grains, which are parallel to each other leaving a susceptible weld centre line. The long straight-sided columnar grain structure becomes weaker under stress or shrinkage strains than the more equiaxed, finer grain structure produced by slow welding speeds. It is essential to know that the coarser the cell structure, the higher the segregation. High welding speeds produce finer cell spacings than slow welding speeds. The dendritic growth in weld metals is the result of high constitutional supercooling, which is greater at the end craters [5, 6, 7].

3.6.2 Segregation species

Segregation in weld solidification can be controlled to some extent by alloy additions. Segregation occurs due to partitioning of elements. The amount of segregation principally depend on the partitioning co-efficient k given by,

$$k = X_S / X_L$$

X_S - mole fraction of solute in solid at given temperature

X_L - mole fraction of solute in liquid at given temperature

Different alloy elements have different k values, where greater partitioning takes place with a smaller k value.

Element	k, Value
Al	0.92
B	0.05
C	0.13
Cr	0.95
Co	0.90
Cu	0.56
H	0.32
Mn	0.84
Mo	0.80
Ni	0.80
N	0.28
O	0.02
P	0.13
Si	0.66
S	0.02
Ti	0.14
W	0.95
V	0.90

Table 3.6.2 : ***Estimation of the partition coefficient of elements in δ iron [5].***

Of these elements, sulphur is often considered to be the most dangerous because it readily forms (Mn Fe)S with iron and manganese, a compound of low melting point which easily spreads along the grain boundaries. Segregation causes high constitutional super cooling which produces a coarser cellular - dendritic structure. As

mentioned earlier, high segregation levels and relatively small temperature gradients give the largest amount of constitutional super cooling.

3.6.3 Residual Stresses and Joint Geometry

The thermal cycle of the weld process always results in residual stresses left in the weld. The severity of these stresses depends on the degree of restraint offered by the weld joint which in turn is control led by the joint geometry. Thicker or stronger plates have higher restraint than thin plates hence greater the residual stresses are left in the weld.

3.6.4 The Mechanism of Solidification Cracking

The partition and rejection of alloying elements at columnar grain boundaries cause marked segregation as shown in Figure 3.6.4. The segregants form low melting phases or eutectics in the form of highly wetting films at grain boundaries. These films weaken the structure to the extent that cracks form at the boundaries under the influence of the tensile residual stresses that occur during cooling of the weld. Impurities or alloying elements causing solidification cracking have the following characteristics:

(1) A low partition co-efficient, k

(2) Compounds have low melting point or form eutectics with the base metal

(3) Readily form compounds with metal

(4) Have a low 'wetting angle' with the metal and thus possess the ability to spread along grain boundaries

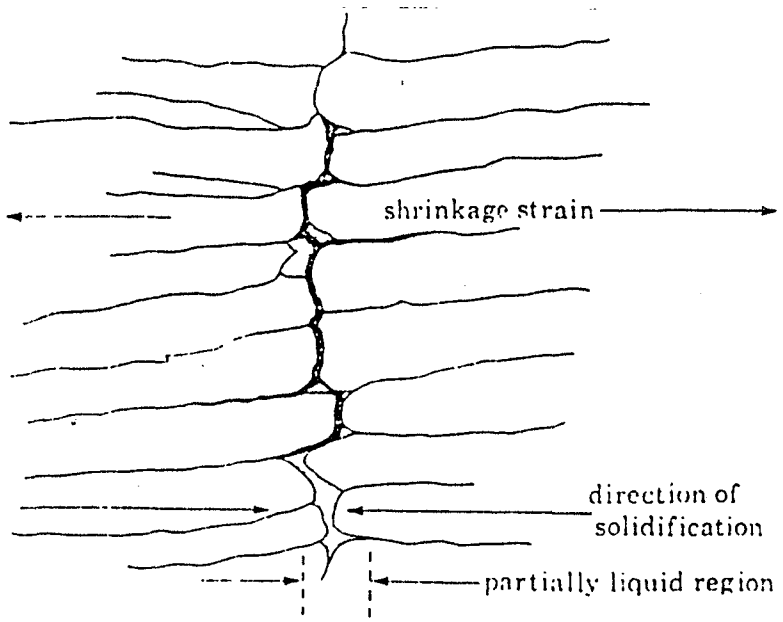

Figure 3.6.4 : ***The mechanism of solidification cracking [12].***

Any alloying process that reduces the effect of segregation impurities to a minimum is always considered advantageous. For example: Addition of Mn forms MnS instead of FeS, which is usually beneficial. FeS has a much lower wetting angle than MnS, so it forms inclusions rather than grain boundary films. MnS has a higher freezing temperature than FeS (1600°C compared to 1190°C). The mechanism by which

solidification cracking occurs is one in which cracks nucleate at liquid or semi liquid sulphide matrix interfaces and spread along the boundary under the influence of tensile thermal stresses [5, 7].

Chapter Four

4.0 EXPERIMENTAL METHODS AND MATERIALS

4.1 INTRODUCTION

In the Australian pipeline industry thin walled X80 pipe grade steel can provide substantial cost savings in materials and service reliability. But these benefits can only be achieved if appropriate consumables are available to match the X80 steel. The cellulosic electrodes used in pipeline welding have proven to be a key economical factor as they offer better arc stability and root penetration even at high travel speed.

Effective laboratory simulation of pipeline welding has been the subject of debate over many years. A variety of test has been proposed to test the cracking propensity of weld metal. Over the years, external restraint tests and self restraint tests were performed to characterise hydrogen assisted cold cracking (HACC), however most of the tests developed induce cracks which are confined to the heat affected zone (HAZ). Due to advancement in steel making, cracking in pipeline steels typically occurs in the weld metal. The effect of weld eccentricity on bending and local stresses at the weld root is shown in Figure 4.1. The Lehigh slot test has been used to simulate cracking in weld metal as local bending moments arising from eccentricity of the weld deposit relative to the plate centreline induce transverse tensile stress at the root of the weld (Figure 4.1.b). High root stress tends to promote HAZ cracking in steels that have high carbon equivalent (CE).

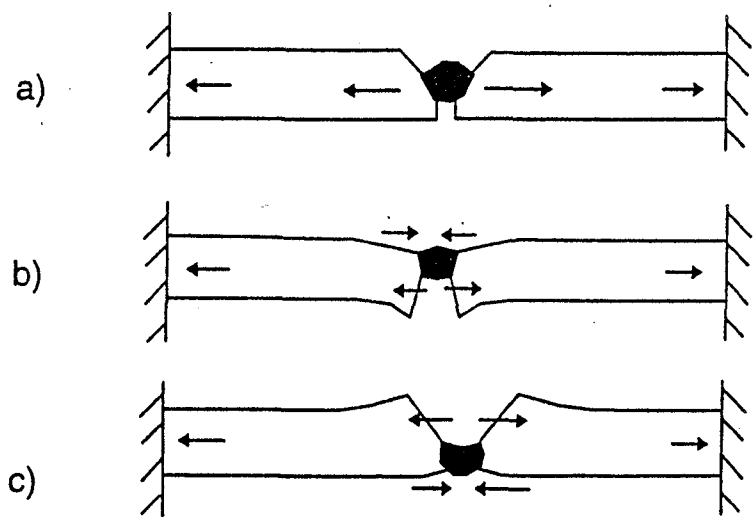

Figure 4.1: ***Effect of weld eccentricity on bending moment and local stress at weld root face (a) Tekken test (b) Lehigh test (c) WIC test [12].***

The Tekken cracking test has also been used widely, but it fails to simulate the joint configuration and bending moments in actual pipeline girth welds subjected to lifting stress as shown in Figure 4.1.a. Although the rigid restraint cracking test (RRC) allows simulation of the joint configuration, it is difficult to apply preheat and appropriate restraint intensity. The Welding Institute of Canada (WIC) restraint

cracking test offers some advantages over the other tests for simulating pipeline welding stress conditions. In this test, the restraint force and the local stress tend to induce cracking on the surface of the weld deposit as shown in Figure 4.1.c. In real pipeline welding, the surface of the weld deposit at the 6 o'clock position experiences a similar force during lifting and lowering operations. The test configuration is simple and offers a range of restraint intensities (by changing restraint lengths) conducted at different preheat and precool temperatures. The WIC test was selected for the present investigation.

4.2 MATERIALS AND CONSUMABLES

X80 steel strip with 8.5mm thickness was used as the weld testing plate. The X80 grade alloy design is based on C-Mn-Nb-Ti alloying system and has a low carbon content, and a restricted CE. The chemical composition of the X80 steel shown in Table 4.2.1. The joint preparation was in accordance with API guidelines and details of the dimensions are showed in Figure 4.2.1 [13].

All test welds were deposited using the shielded metal arc welding process in the vertical down position with 4mm diameter cellulosic electrode. Five different brands of commercial electrodes with two different strength levels (E9010 and E6010) were investigated. Chemical composition of X80 steel is shown in Table 4.2.1.

Elements	Weight Percentage (%)
C	0.060
P	0.012
Mn	1.59
Si	0.27
S	0.004
Ni	0.026
Cr	0.016
Mo	0.23
Cu	0.009
Al	0.29
Sn	0.002
Nb	0.051
V	0.004
Ti	0.012
B	< 0.0003
Ca	0.00007

Table 4.2.1: *Chemical Composition of X80 Steel*

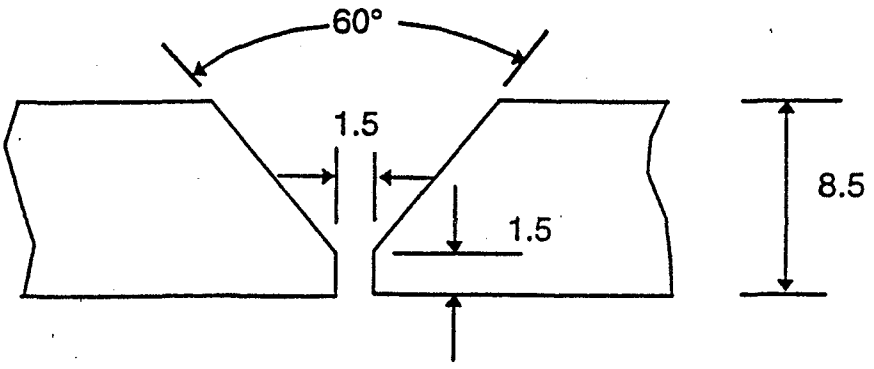

Figure 4.2.1: *API joint preparations for pipeline welding, All dimensions in mm.*

4.3 WIC RESTRAINT CRACKING TEST

The WIC restraint cracking test was developed by the Welding Institute of Canada to measure the susceptibility of weld metal cracking in pipeline girth weld and is widely used for the assessment of welding performance. The testing method utilises a backing plate on which the test plate is restrained by welding along the sides. The free length (L) of the test plate at the centre constitutes the restraint length of the test set up which influences restraint intensity of the joint. The backing plate is further welded to a web to achieve an appropriate restraint intensity. The dimensions of the test set up are also shown in Figure 4.3.1.

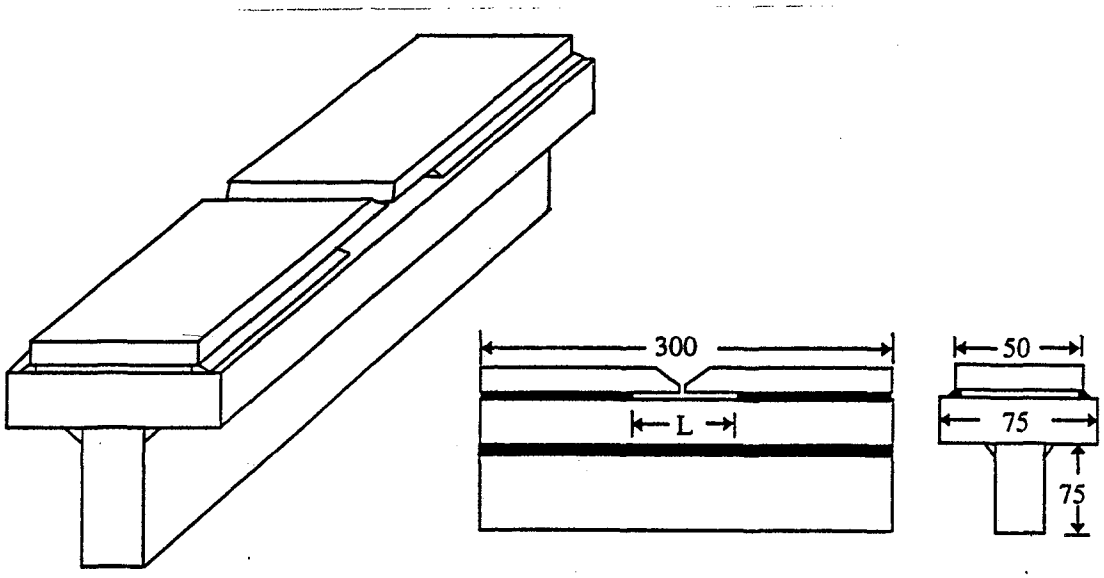

Figure 4.3.1: ***WIC restraint cracking test set up and dimensions (mm) [12].***

Most of the tests were carried out at room temperature(20 – 22°C). Cracking in the weld metal is greatly influenced by hydrogen content which depends on the cooling rate of the weld. The effect of cooling rate on cracking was examined by preheating the test blocks to various temperatures. The restraint intensity was held constant using a standard restraint length of 25mm.

4.4 WELDING PARAMETERS AND PREPARATION

A single root pass weld was deposited in the vertical down position using DC electrode positive. Different preheat temperatures were employed between 22 – 100°C to investigate the crack sensitive critical preheat temperature. The welding parameters are shown in Table 4.4.1.

Current (amps)	Voltage (volts)	Travel Speed (mm / min)	Heat Input (kJ / mm)	Restraint Length (mm)	Preheat Temp (°C)
128 - 140	23 - 30	250 - 430	0.45 - 1.0	25	22 - 40

Table 4.4.1: ***Welding parameters used for the weld deposited in WIC restraint cracking test.***

In most of the welding tests, the cooling time was determined by platinum or platinum – rhodium thermocouples plunged into the moving molten pool behind the arc. Some tests were strain gauged to determine the onset time of cracking and, in addition a clip

gauge was attached to monitor elastic and plastic strains during solidification of the weld.

4.5 PREPARATION OF TEST SAMPLES

Preparation of test samples included sectioning, polishing, grinding and etching. The test samples are extracted from the test rig after 24 hours by saw cuts.

(1) **Sectioning** - each sample was sectioned perpendicular to the weld into 4 conveniently sized pieces. This is one of the major operations in the preparation of metallographic specimen.

(2) **Grinding** - the four sections from each sample were polished using P240, P320, P400, P600, P1200, P2400 and P4000 grit papers on a glass surface until all scratches from the previous stage had disappeared from the surface.

(3) **Polishing** - was carried out using 6 micron then 1 micron diamond pads.

(4) **Etching** - was carried out with 2.5% Nital solution. After etching the sections were microscopically examined for HACC and solidification cracks.

4.5.1 Preparation of samples for Scanning Electron Microscope Analysis:

Fracture surfaces of HACC and solidification cracked samples were examined by SEM. Samples were first sliced to 2 – 5mm thick sections. The thin slices of the sections were then frozen in liquid nitrogen for about 5 to 10 minutes and then they were cracked open using a hammer to reveal the fracture surface. The fractured

specimen was then ultrasonically cleaned and subsequently used for SEM examination. In some of the specimens an attempt was made to correlate the microstructure with the cold cracked and hot cracked fracture surface.

4.6 HARDNESS TESTING

Microhardness testing was carried out for all the different brands of electrode used for the WIC test. Profiles of microhardness measurements on surfaces of samples revealed hardness distributions in various constituents such as weld metal, HAZ and base metal. The data obtained through microhardness testing are discussed in the following chapter

Chapter Five

5.0 EXPERIMENTAL RESULTS

5.1 WIC Restraint Test Results:

Four brands of commercial E9010 electrodes were investigated which are referred to as Electrodes A, B, C, and D. The welding parameters for vertical downward welding are shown in Table 5.1.1.(a, b, c, d). Also three brands of commercial E6010 electrodes were investigated which are referred as Electrodes A_1, B_1 and C_1. The welding parameters for the E6010 electrodes are given in table 5.1.2. (a, b, c).

No	Travel Speed mm/min.	Heat Input kJ/ mm	Preheat Temperature T_p in $^{\circ}C$
1	342	0.6	22 - 24
2	248	0.89	22 - 24
3	366	0.61	22 - 24
4	438	0.48	30
5	333	0.57	35
6	286	0.74	35
7	365	0.55	40
8	291	0.67	40
9	267	0.72	40

Table 5.1.1 (a): ***Welding parameters for electrode A (E9010) at different preheat temperatures.***

No	Travel Speed mm / min	Heat Input kJ / mm	Preheat Temperature T_p °C
1	480	0.43	22 - 24
2	333	0.61	30
3	405	0.52	30
4	333	0.65	35
5	382	0.56	35

Table 5.1.1 (b) : ***Welding parameters for electrode B (E9010) at different preheat temperatures.***

No	Travel Speed mm / min	Heat Input kJ / mm	Preheat Temperature T_p °C
1	272	0.74	22 - 24
2	461	0.47	30
3	308	0.66	30
4	375	0.56	35
5	357	0.55	40
6	313	0.60	40

Table 5.1.1 (c): ***Welding parameters for electrode C (E9010) at different preheat temperatures.***

No	Travel Speed mm / min	Heat Input kJ / mm	Preheat Temperature T_p °C
1	300	0.71	22 - 24
2	339	0.59	22 - 24
3	344	0.59	30
4	338	0.61	30
5	242	0.82	35
6	338	0.63	35
7	303	0.66	40
8	408	0.50	40

Table 5.1.1 (d) : ***Welding parameters for electrode D (E9010) at different preheat temperatures.***

No	Travel Speed mm / min	Heat Input kJ / mm	Preheat Temperature T_p °C
1	316	0.65	22 - 24
2	319	0.70	22 - 24
3	408	0.57	22 - 24
4	405	0.54	30
5	327	0.65	30
6	336	0.55	30

Table 5.1.2 (a) : ***Welding parameters for electrode A_1 (E6010) at different preheat temperatures.***

No	Travel Speed mm / min	Heat Input kJ / mm	Preheat Temperature T_p °C
1	397	0.57	22 - 24
2	359	0.64	22 - 24
3	285	0.79	30
4	440	0.50	30

Table 5.1.2 (b) : ***Welding parameters for electrode B_1 (E6010) at different preheat temperatures.***

No	Travel Speed mm / min	Heat Input kJ / mm	Preheat Temperature T_p °C
1	353	0.61	22 - 24
2	341	0.65	22 - 24
3	359	0.61	30

Table 5.1.2 (c) : ***Welding parameters for electrode C_1 (E6010) at different preheat temperatures.***

All the tests carried out with both E9010 and E6010 grades were with constant restraint length of 25mm (R_L). The principle behind employing different preheat temperatures is to determine the critical crack sensitive preheat temperature for each brand of electrode investigated.

5.2 CHEMICAL ANALYSIS OF DILUTED WELD METAL

Chemical analysis was carried out by atomic emission spectroscopy and the composition of the 4 samples of diluted E9010 grade and 3 samples of E6010 are shown in Table 5.2.1. All of the elements are reported in weight %.

ELEMENT	Electrode A	Electrode B	Electrode C	Electrode D
Mn	1.26	1.02	1.06	1.29
Si	0.22	0.18	0.16	0.26
Ni	0.32	0.28	0.35	0.34
Cr	0.020	0.023	0.022	0.018
C	0.110	0.135	0.130	0.145
Mo	0.41	0.14	0.19	0.23
Cu	0.010	0.011	0.031	0.011
Al	0.013	0.007	0.011	0.013
Sn	0.003	< 0.002	0.004	0.008
Nb	0.032	0.020	0.022	0.040
Ti	0.016	0.013	0.012	0.021
V	0.0040	0.032	0.006	0.006
B	0.0004	<0.0003	<0.0003	<0.0003
Ca	0.0005	0.0005	0.0005	<0.0005
N	0.0047	0.0057	0.0056	0.007
O	0.050	0.061	.0635	0.040
P	0.013	0.014	0.015	0.016
S	0.006	0.005	0.007	0.011
CE	**0.43**	**0.36**	**0.38**	**0.43**

Table 5.2.1 : ***Chemical compositions of diluted E9010 weld metal for four different brands of electrode.***

ELEMENT	Electrode A_1	Electrode B_1	Electrode C_1
C	0.105	0.130	0.100
Mn	1.20	1.40	1.16
Si	0.24	0.33	0.25
Ni	0.024	0.030	0.028
Cr	0.015	0.027	0.019
Mo	0.14	0.17	0.16
Cu	0.010	0.018	0.011
Al	0.012	0.020	0.015
Sn	0.003	0.007	0.006
Nb	0.028	0.045	0.041
Ti	0.020	0.027	0.019
V	0.004	0.006	0.007
B	<0.0003	0.0003	<0.0003
Ca	0.0005	0.0005	0.0005
N	0.0036	0.0051	0.0043
O	0.049	0.044	0.0462
P	0.015	0.015	0.018
S	0.007	0.011	0.013
CE	**0.34**	**0.410**	**0.34**

Table 5.2.2. : ***Chemical compositions of diluted E 6010 weld metal for three different brand of electrodes.***

Based on all-weld metal compositional analysis, all of the diluted weld metals of E9010 showed increased manganese (Mn) percentage after dilution. The increase in

Mn increases the acicular ferrite content in the microstructure. It also resulted in lower CE due to reduction in other alloy contents such as (Mo and Ni). Since dilution and heat input are proportional to each other, E 9010 consumables at low heat input overmatch the X 80 pipe steel strength. The strength also depends on the CE of the individual electrode as well. Table 5.2.2. show the chemical compositions for diluted weld metal of the three E6010 commercial electrodes. Due to the high dilution of weld metal with the X80 base (about 50%), even under matching electrodes such as E 6010 can be close to matching the strength of the pipe steel.

5.3 DETERMINATION OF CRITICAL PREHEAT TEMPERATURE

The test matrix of WIC restraint tests (Table 5.3) outlines the cracking behaviour of each brand and grade of electrode with respective preheat temperatures. Although the tests carried out for preheat temperatures of 60°, 80° and 100° are not included in this thesis, it is essential to mention the results to determine the critical crack free temperature. Test blocks preheated to 40°, 60°, 80° and 100° C showed no cracking in the weld metal and thus it became critical to carefully analyse the remaining tests at preheat temperatures of 30° and 35° C.

Preheat Temperature°C	22	30	35	40	60	80	100
Electrode A E 9010	C	C	C	UC	UC	UC	UC
Electrode B E 9010	C	C	C	UC			
Electrode C E 9010	C	C	C	UC	UC	UC	UC
Electrode D E 9010	C	C	C	UC			
Electrode A_1 E 6010	C	UC					
Electrode B_1 E 6010	C	UC					
Electrode C_1 E 6010	C	UC					

C - Cracked UC - Uncracked Shaded - Tests not carried out

Table 5.3 : ***WIC Restraint cracking test matrix.***

5.3.1 Cracking in E 9010 Electrodes

Electrodes A, B, C and D showed cracking at preheat temperatures 22°C and 30°C. But only partial cracking was observed at a preheat temperature of 35°C and no cracking was evident at 40°, 60°, 80°and 100°C. Despite the narrow band of CE (0.30 - 0.43) among the electrodes, it can be concluded that crack free welds are produced with strength matching E 9010 consumables at 40° C. Figure 5.3.1 shows the macrophotographs of weld metal produced from E 9010 electrodes at preheats of 35°C and 40°C.

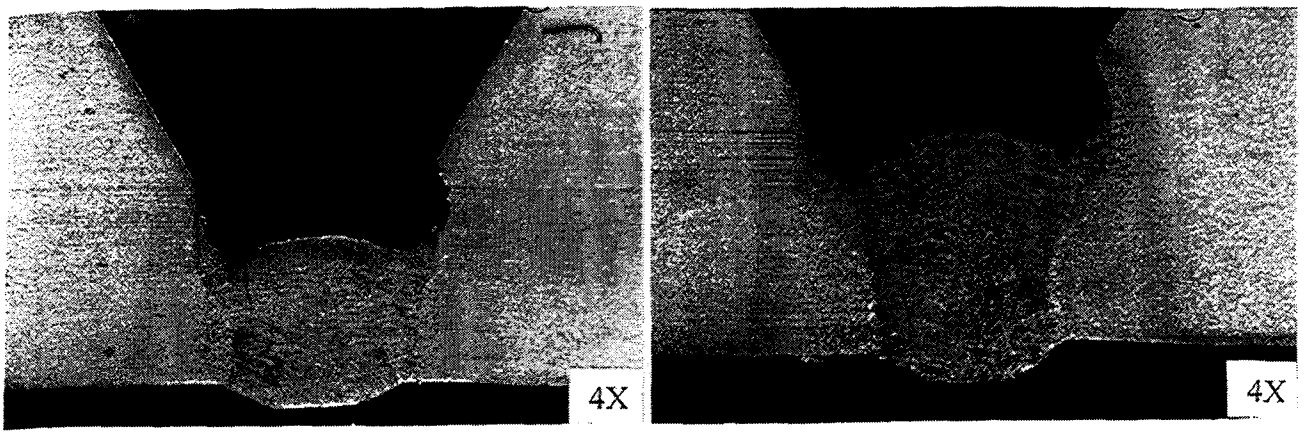

[a] [b]

Figure 5.3.1 : ***Macrophotographs of weld metal from E 9010 electrode A. (a) 35°C and (b) 40°C.***

5.3.2. Cracking Behaviour in E 6010 Electrodes

Undermatching electrodes also showed similar cracking results at room temperature. However, they did not show any cracking at a preheat temperature of 30°C. So it was concluded that crack-free welds are produced with E 6010 grade electrodes at 30°C. Figure 5.3.2. shows macrophotographs of E 6010 electrode weld metals at 22°C and 30°C.

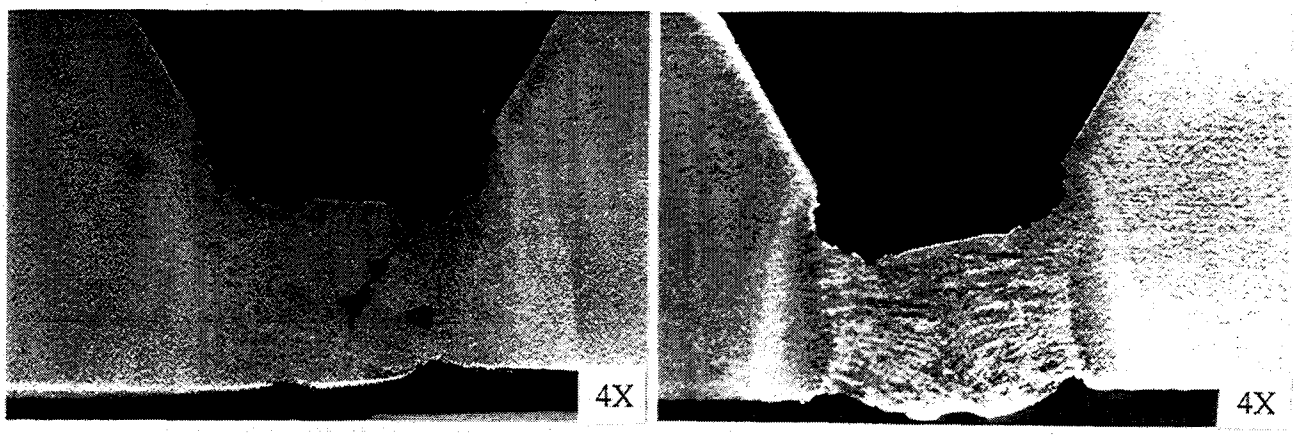

[A] [B]

Figure 5.3.2 : ***Macrophotographs of E 6010 electrode B_1, (A) 22°C and (B) 30°C***

5.4 CRACKING PERCENTAGE

It is essential to investigate the percentage of cracking for each brand of electrode. However, there is a variation in performance from manufacturer to manufacturer and in the worst case from batch to batch. Magnification affects the ability to determine the cracking percentage values. The correlation between the CE and cracking percentage was examined, where the percentage cracking was evaluated by the formula:

$$C\% = [(C_1 / L_1 + C_2 / L_2 + C_3 / L_3 + C_4 / L_4) / 4] * 100$$

C_1 C_2 C_3 C_4 - length of the crack in each of the four sample section

L_1 L_2 L_3 L_4 - leg length of the weld (Figure 5.5.1)

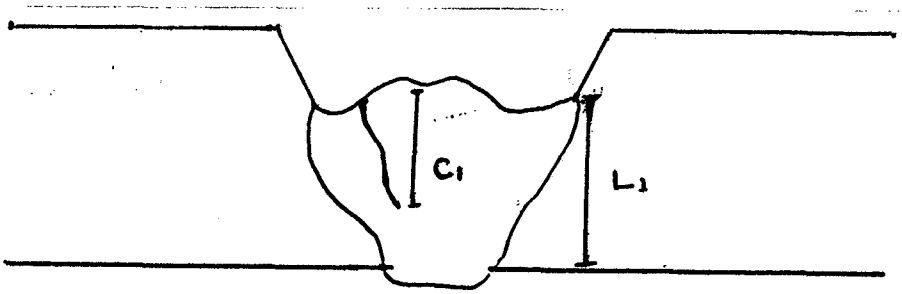

Figure 5.4.1 : ***Diagrammatic illustration of calculating cracking percentage.***

In certain sections of the sample, unequal leg lengths were also experienced. In such instances, the mean leg length was taken to calculate the percentage of cracking.

Figure 5.4.2 shows the cracking percentages for E 9010 electrodes at different preheat temperatures. From the figure it is understood that at higher preheat the incidence of cracking is reduced. Higher preheat temperatures ensure slower cooling rates which allows enough time for hydrogen to effuse from the weld metal.

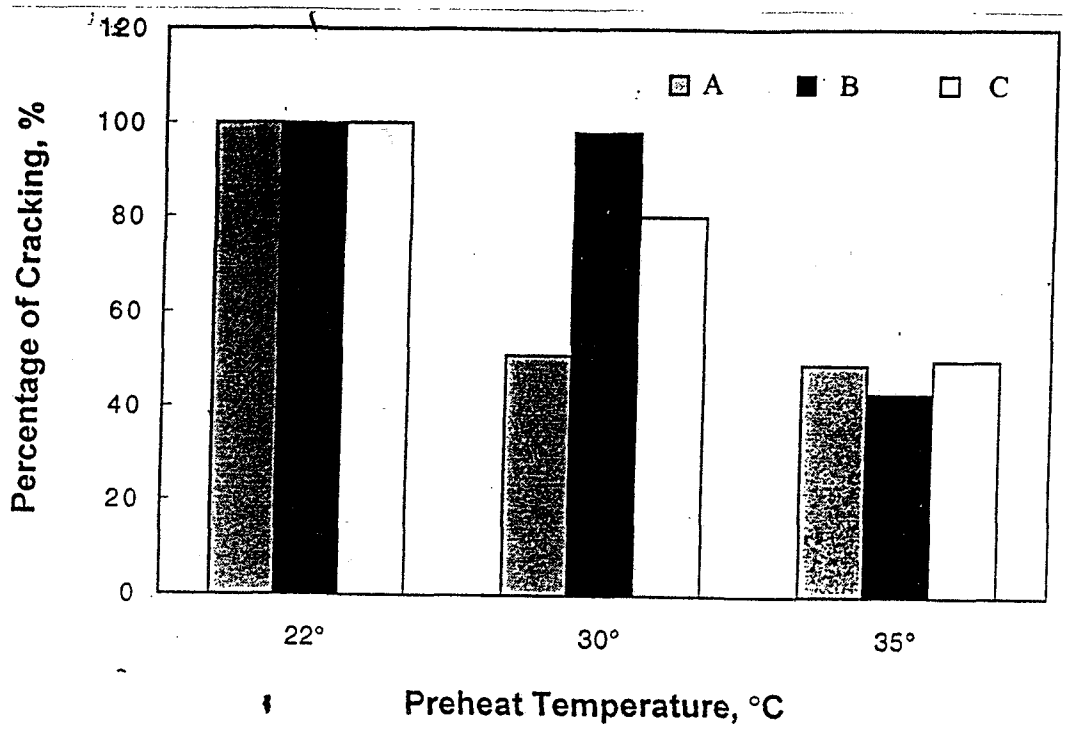

Figure 5.4.2 : *Cracking percentage for E 9010 electrodes.*

A preheat of 40°C or more was found to be effective in avoiding HACC in E 9010 electrodes at low heat inputs of 0.50 kJ / mm. A preheat of 30°C was effective in avoiding cracking in E 6010 electrodes which also have the advantage of good accommodation of strains induced by residual and thermal stresses during weld cooling.

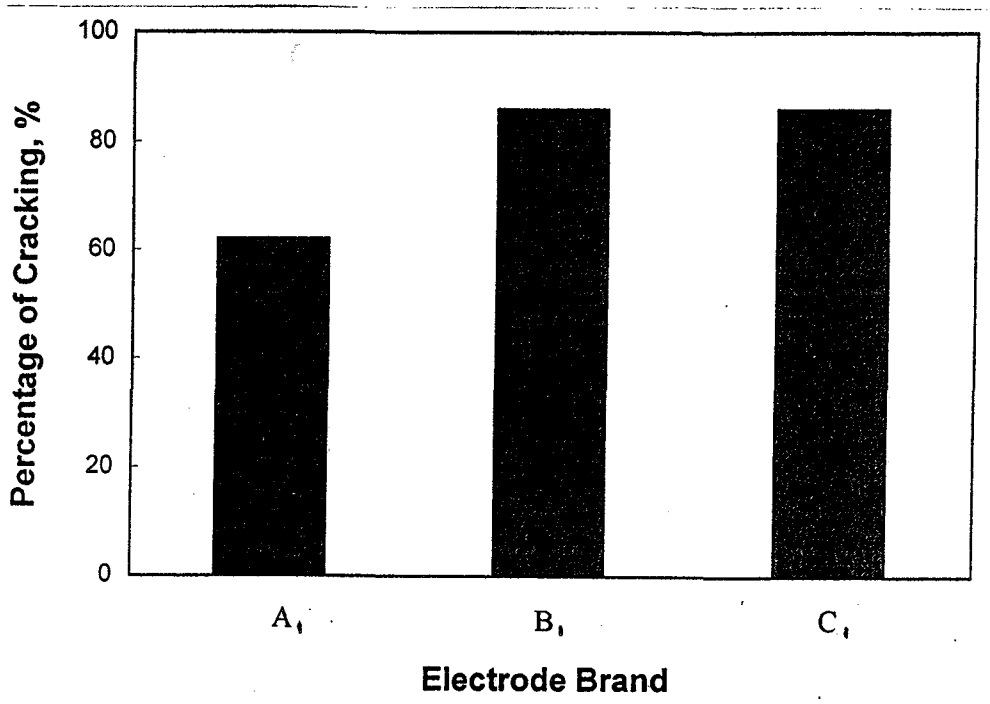

Figure 5.4.3 : ***Cracking percentage for E 6010 electrodes.***

5.5 HARDNESS

Hardness measurements were made using a Vickers hardness tester with a load of 0.5 kg. Hardness values for E 6010 electrodes at a preheat temperature of 22°C and 30°C are shown in Figure 5.5.1. The hardness of the HAZ near the fusion boundary towards the weld metal was found to be higher than for the base metal and weld metal. Also base metal hardness values generally exceeded that of the weld metal. This is due to the fact that the E 6010 electrodes are lower in strength than the X 80 plate. Dilution was not high enough at the low heat inputs of 0.50 - 0.70 kJ / mm to raise the strength and hardness to the base plate values. From the results, it is evident that the

undermatching electrode has produced a softer and coarser microstructure than the base plate.

Average weld metal hardness for the E 9010 and E 6010 electrodes are given in Table 5.5.

Electrode	22°C	30°C	35°C	CE
E 9010 A		270	265	**0.43**
E 9010 B		280	270	**0.36**
E 9010C		258	267	**0.38**
E 9010 D		286	260	**0.43**
E 6010 A_1	252	230		**0.34**
E 6010 B_1	256	239		**0.41**
E 6010C_1	235	210		**0.34**

Table 5.5 : ***Average weld metal hardness for the E 9010 and E 6010 electrodes at different preheat temperatures.***

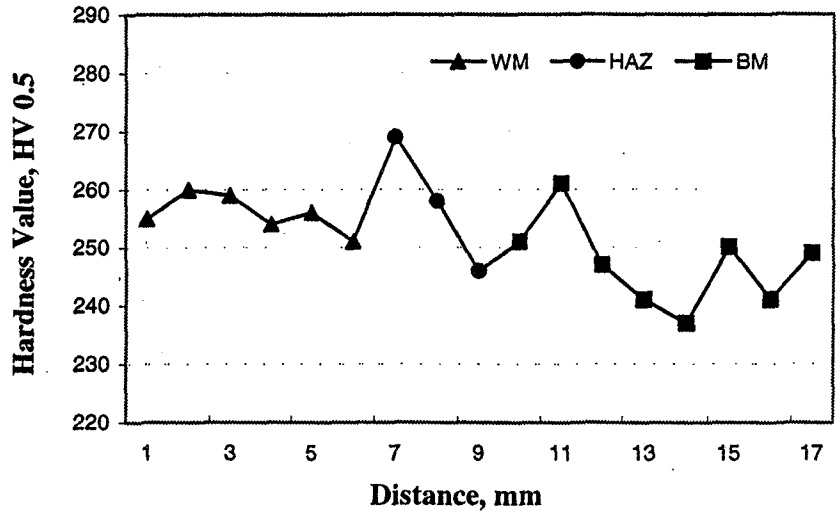

[A]

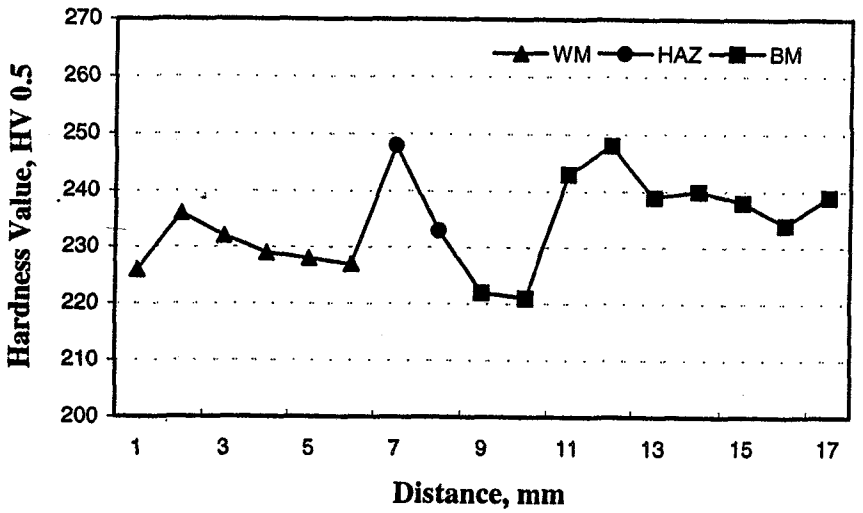

[B]

Figure 5.5.1 (a) : ***Hardness traverse from weld metal to parent metal for E 6010 electrode A_1 (A) 22°C and (B) 30°C***

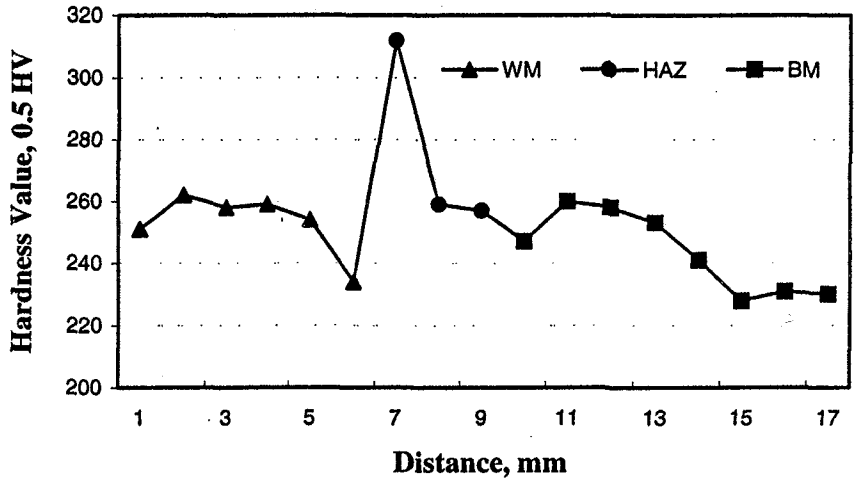

[A]

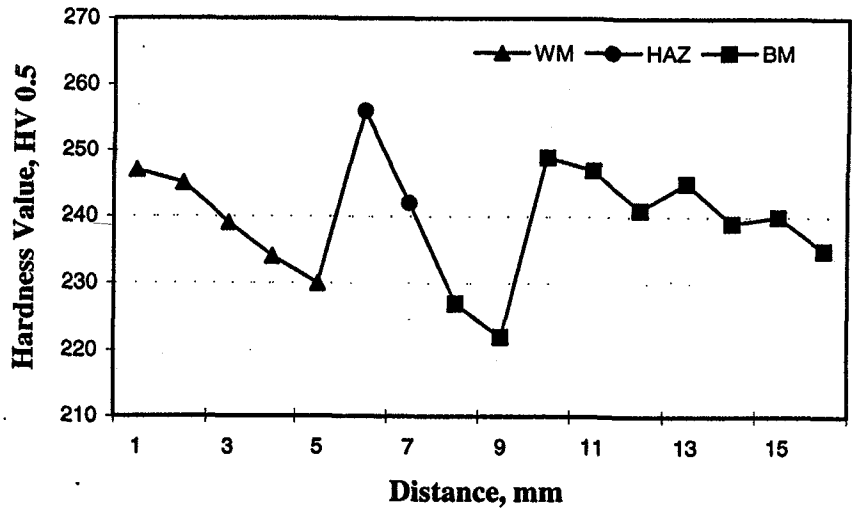

[B]

Figure 5.5.1 (b) : ***Hardness traverse from weld metal to parent metal for E 6010 electrode B_1 (A) 22°C and (B) 30°C.***

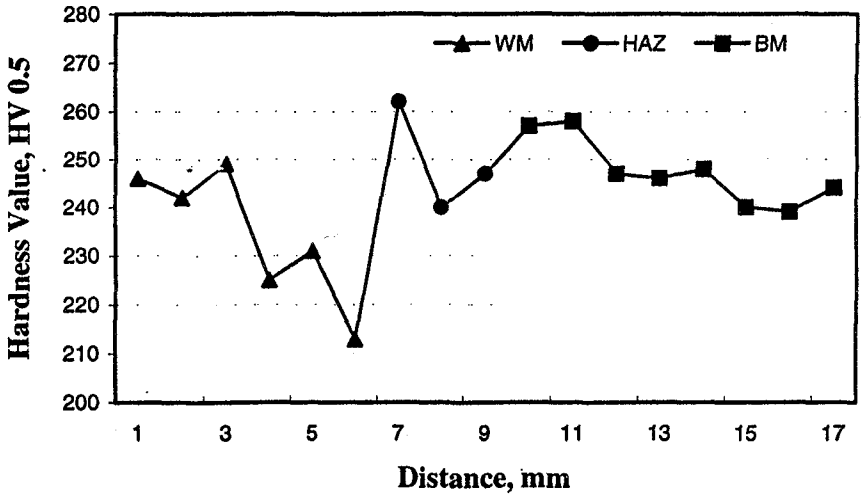

[A]

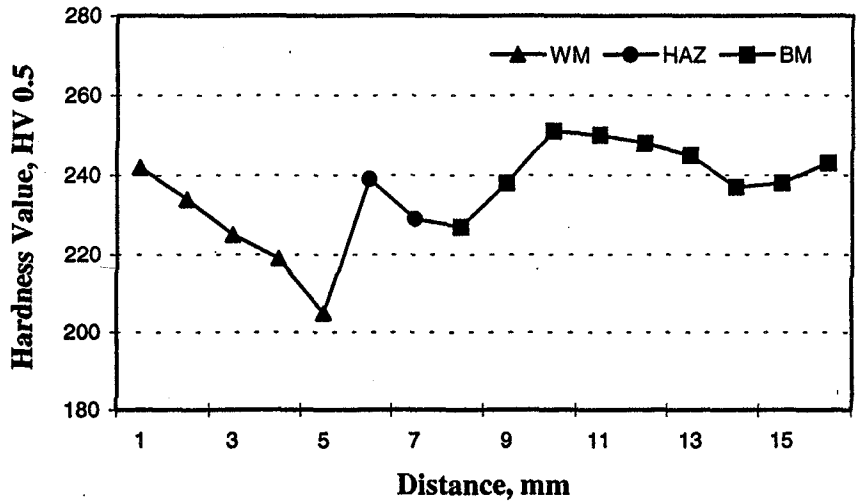

[B]

Figure 5.5.1 (c) : ***Hardness traverse from weld metal to parent metal for E 6010 electrode C_1, (A) 22°C and (B) 30°C.***

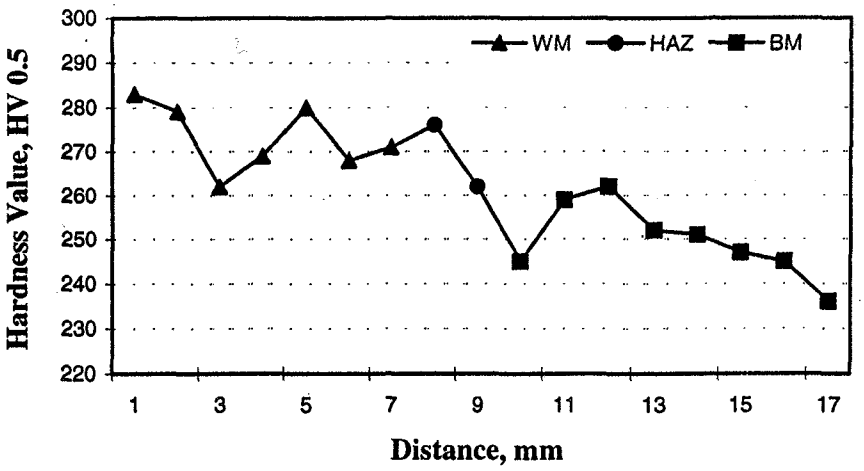

[A]

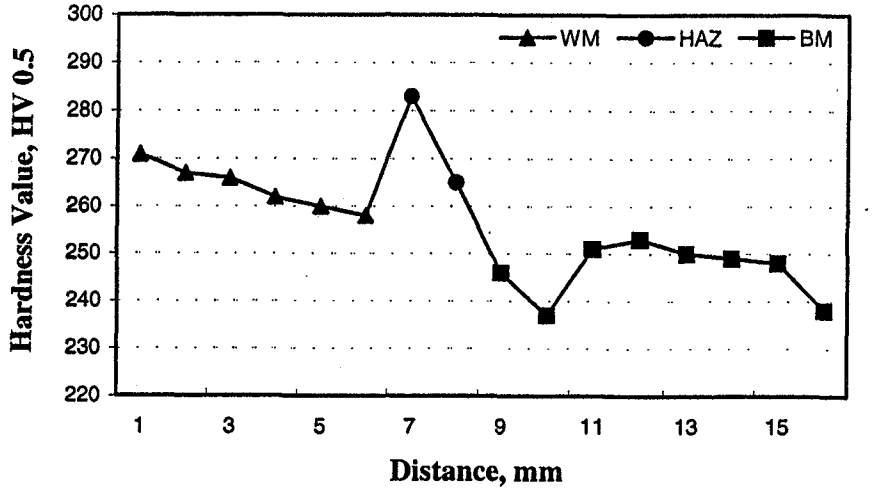

[B]

Figure 5.5.2 (a) : ***Hardness traverse from weld metal to parent metal for E 9010 electrode A, (A) 30°C and (b) 35°C.***

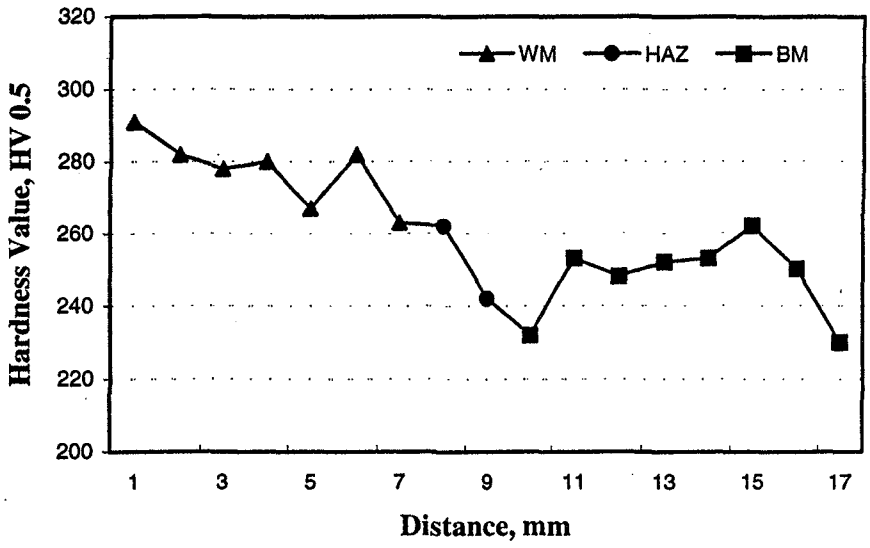

[A]

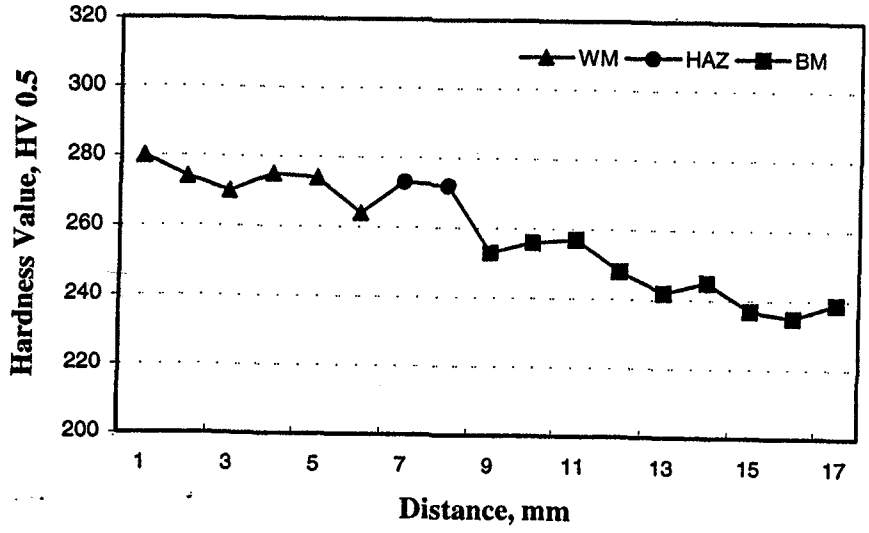

[B]

Figure 5.5.2 (b) : ***Hardness traverse from weld metal to parent metal for E 9010 electrode B, (A) 30°C and (B) 35°C.***

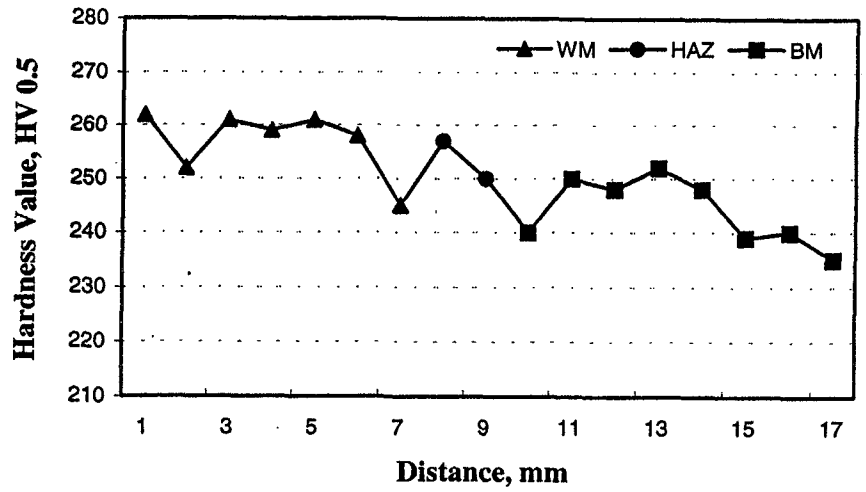

[A]

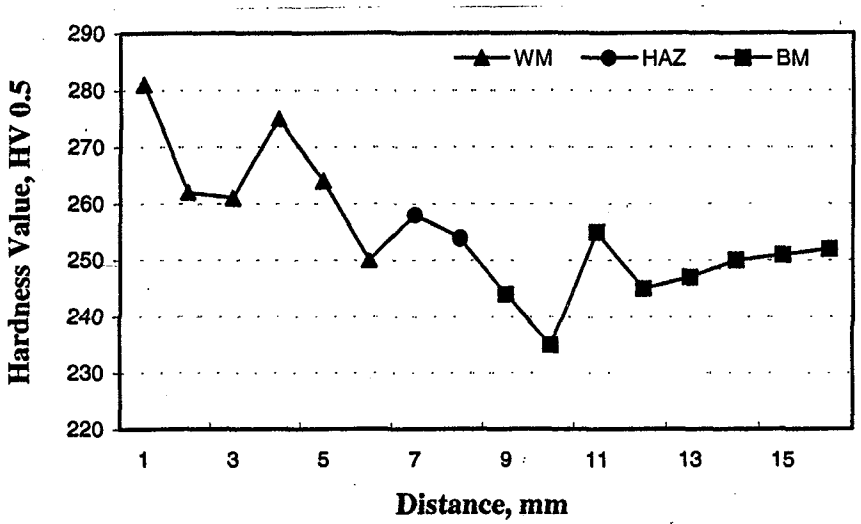

[B]

Figure 5.5.2 (c) : ***Hardness traverse from weld metal to parent metal for E 9010 electrode C, (A) 30°C and (B) 35°C.***

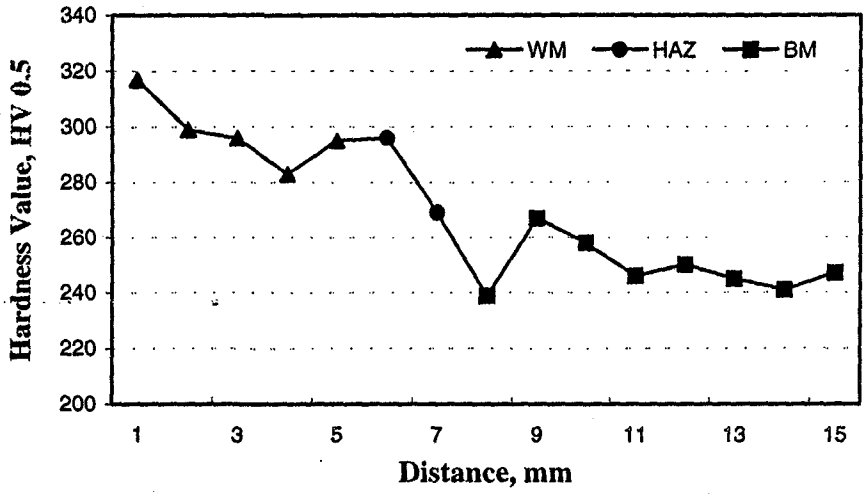

[A]

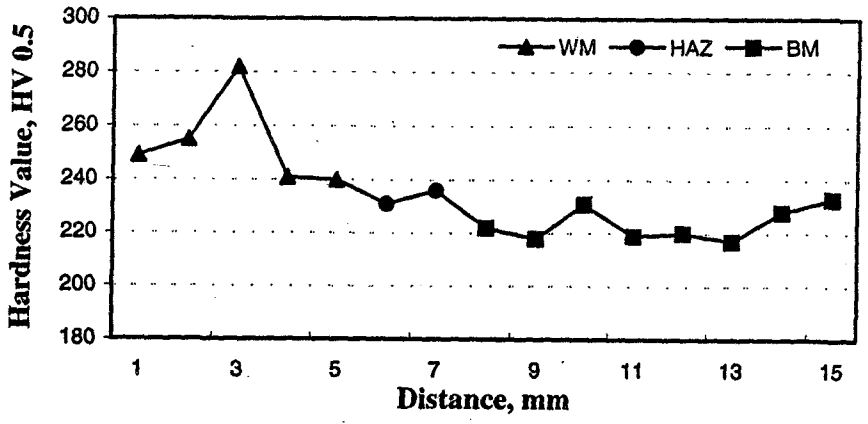

[B]

Figure 5.5.2 (d) : ***Hardness traverse from weld metal to parent metal for E9010 electrode D, (A) 30°and (B) 35°C.***

Hardness values were obtained for E 9010 electrodes A, B, C and D at preheat temperatures 30°C and 35°C, Figure 5.6.2. (a) - (d). The tests on selected samples had a heat input range of 0.47 - 0.71 kJ / mm. Since E 9010 is a higher strength electrode grade than E 6010, the hardness values of the weld metal were found to be higher than both HAZ and parent metal. The relatively low heat inputs result in faster cooling rates which result in a fine microstructure. The higher alloy content of E 9010 electrodes, despite dilution with X 80, increases weld metal hardness above that of X 80. The hardness values for all brands of electrode at different preheat temperatures do not show any systematic trend and therefore hardness values cannot be taken as a predictive tool to determine the likelihood of HACC in the weld metal.

5.6 CRACK ANALYSIS

All test samples extracted from the WIC test block were examined for HACC and solidification cracks. Most of the tests carried out at room temperature showed cracking and the % was calculated using the method outlined in this Section 5.4.

5.6.1 Hydrogen Assisted Cold Crack Analysis

From the selected sections of samples, it is evident that the cause of the crack consisted of grain boundary ferrite, grain interiors with an acicular ferrite structure and the HAZ. The microstructures of weld metal deposited by E 6010 and E 9010

electrodes are shown in Figures 5.6.1.1 and 5.6.1.2 It is evident from the figures that the weld metal from the E 6010 consumable consisted chiefly of columnar grains which are decorated with grain boundary ferrite and ferrite side plates. The microstructures obtained from the weld metal deposited with E 9010 consumable had a substantial amount of grain boundary nucleated ferrite side plates and acicular ferrite in grain interiors.

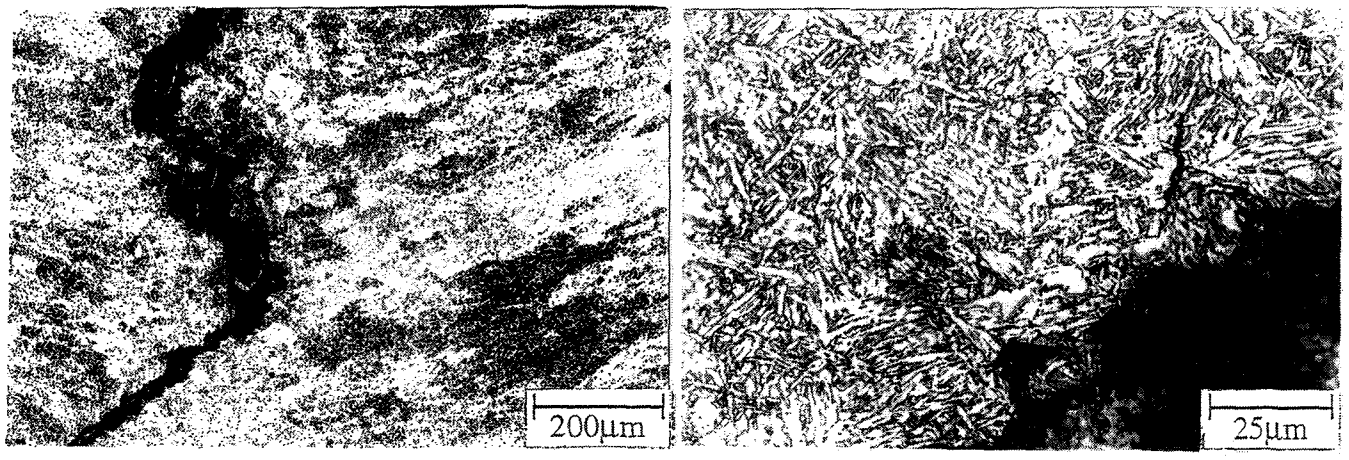

a

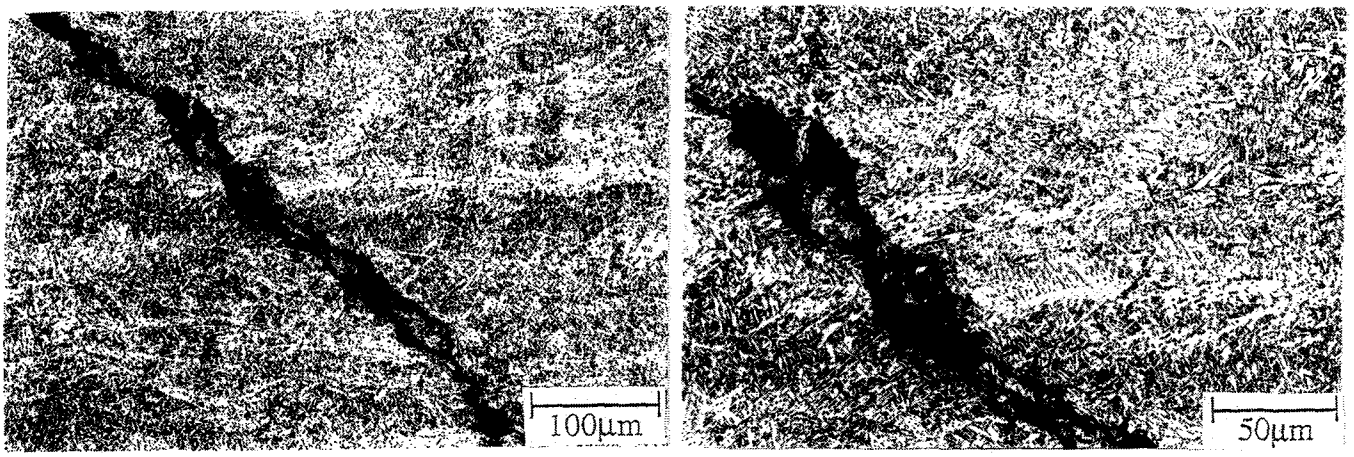

b

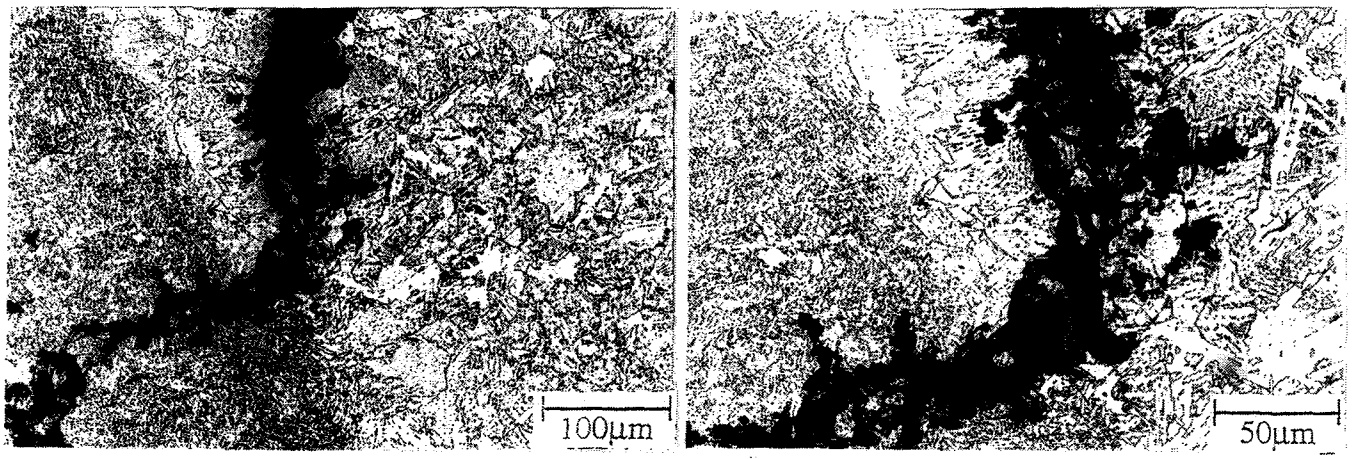

c

Figure 5.6.1.1: ***Microstructures of weld metal deposited from E 6010 electrode.***

[a] and [b] - electrode A_1, [c] - electrode B_1.

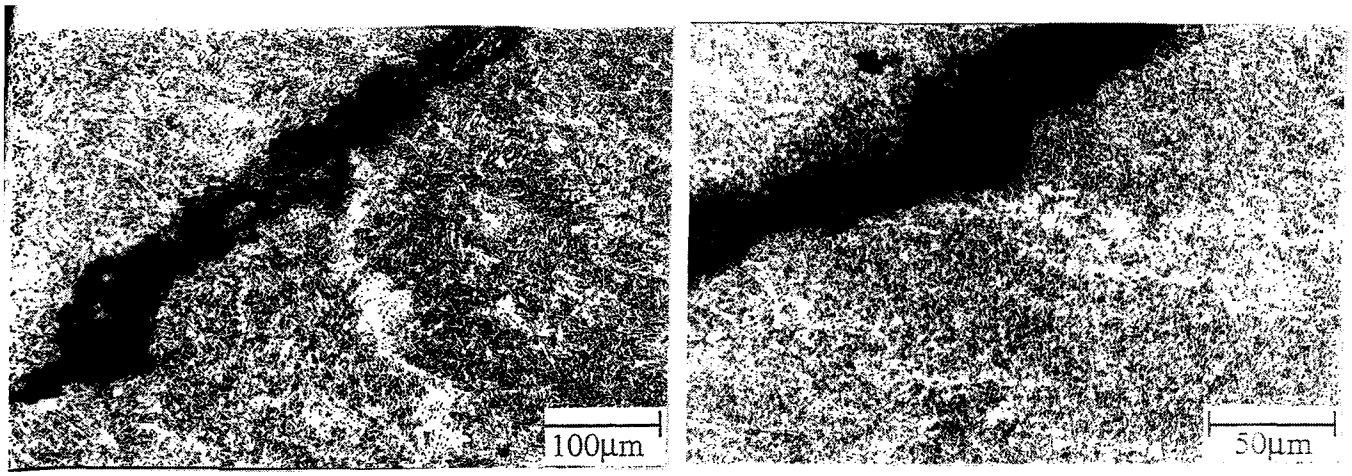

a

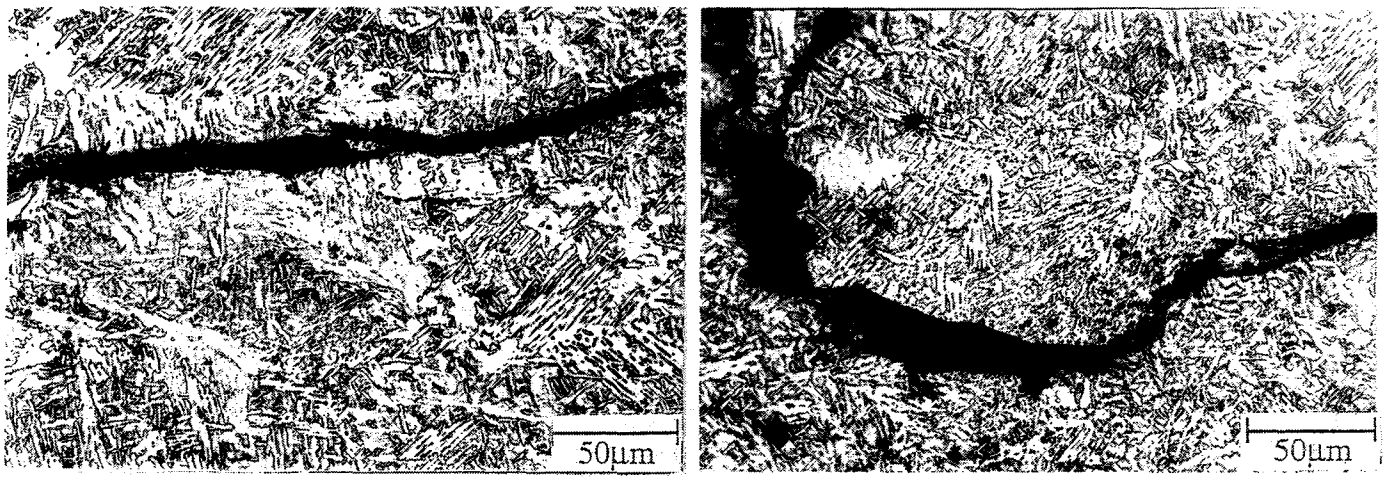

b

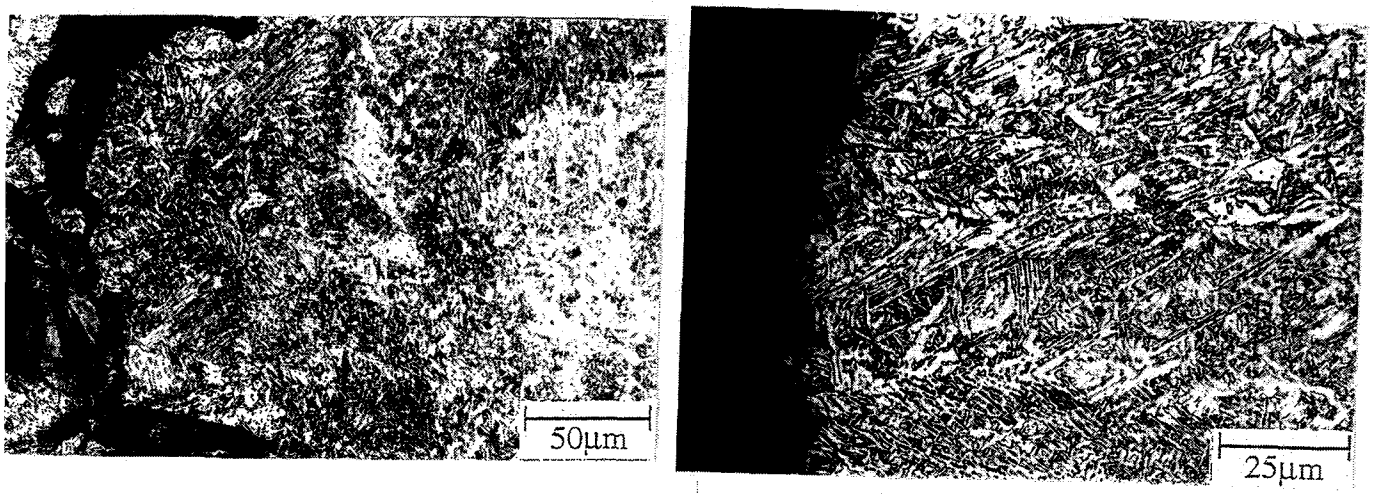

c

Figure 5.6.1.2 : ***Microstructures of weld metal deposited from E 9010 electrode***

[a] - electrode A, [b] - electrode B and [c] electrode D

A macrophotograph of a selected section shown in Figure 5.6.1.3 (a) which illustrates the shape of the weld produced using E 6010 electrode A_1. The enlarged view of the corresponding section is shown in Figure 5.6.1.3 (b). The initiation and early part of cracking occurred in the weld metal and was perpendicular to the columnar grain boundaries. The path of the crack was found to propagate along ferrite veins of columnar grains and some portion across the grain interior which consisted of mainly acicular ferrite.

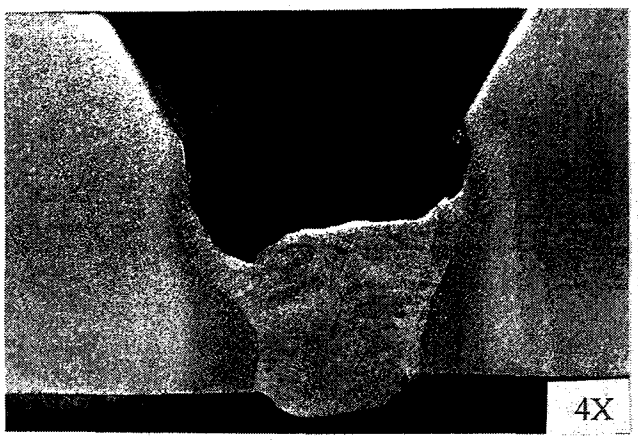

a

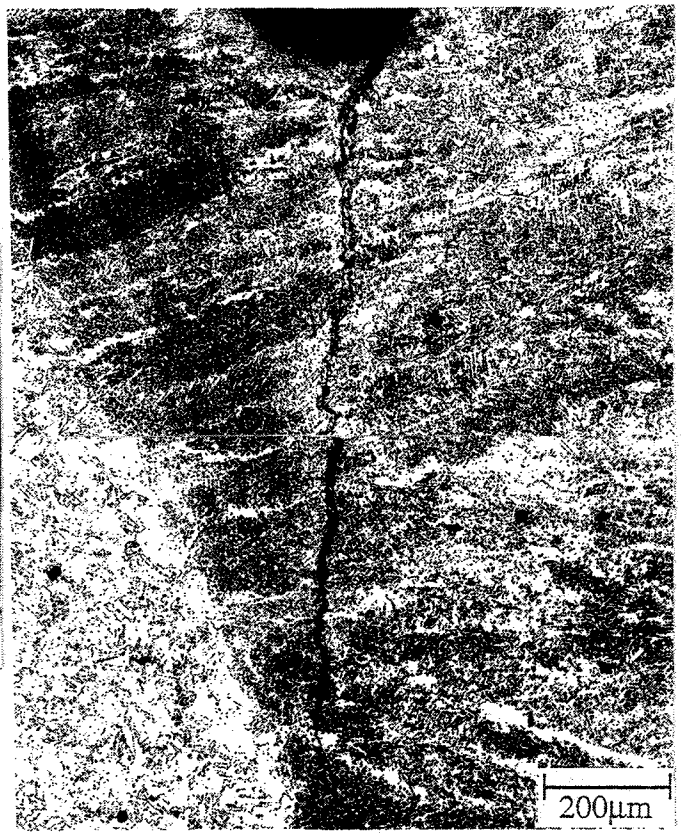

b

Figure 5.6.1.3 : ***(a) Macrophotograph and (b) Enlarged view of the section of weld using E 6010 electrode A_1.***

Relationships between microstructures and the fracture topography of HACC are discussed in the following chapter.

5.6.2 SOLDIFICATION CRACK ANALYSIS

Solidification cracking in weld metal occurred for all electrodes and was most prevalent for tests carried out at room temperature. Figures 5.6.2.1. (a) and (b) show the occurrence of a crack at the centre of the weld metal. The cracks were small and initiated in the weld center and propagated across the columnar grains and across grain interiors consisting of acicular ferrite and ferrite side plates.

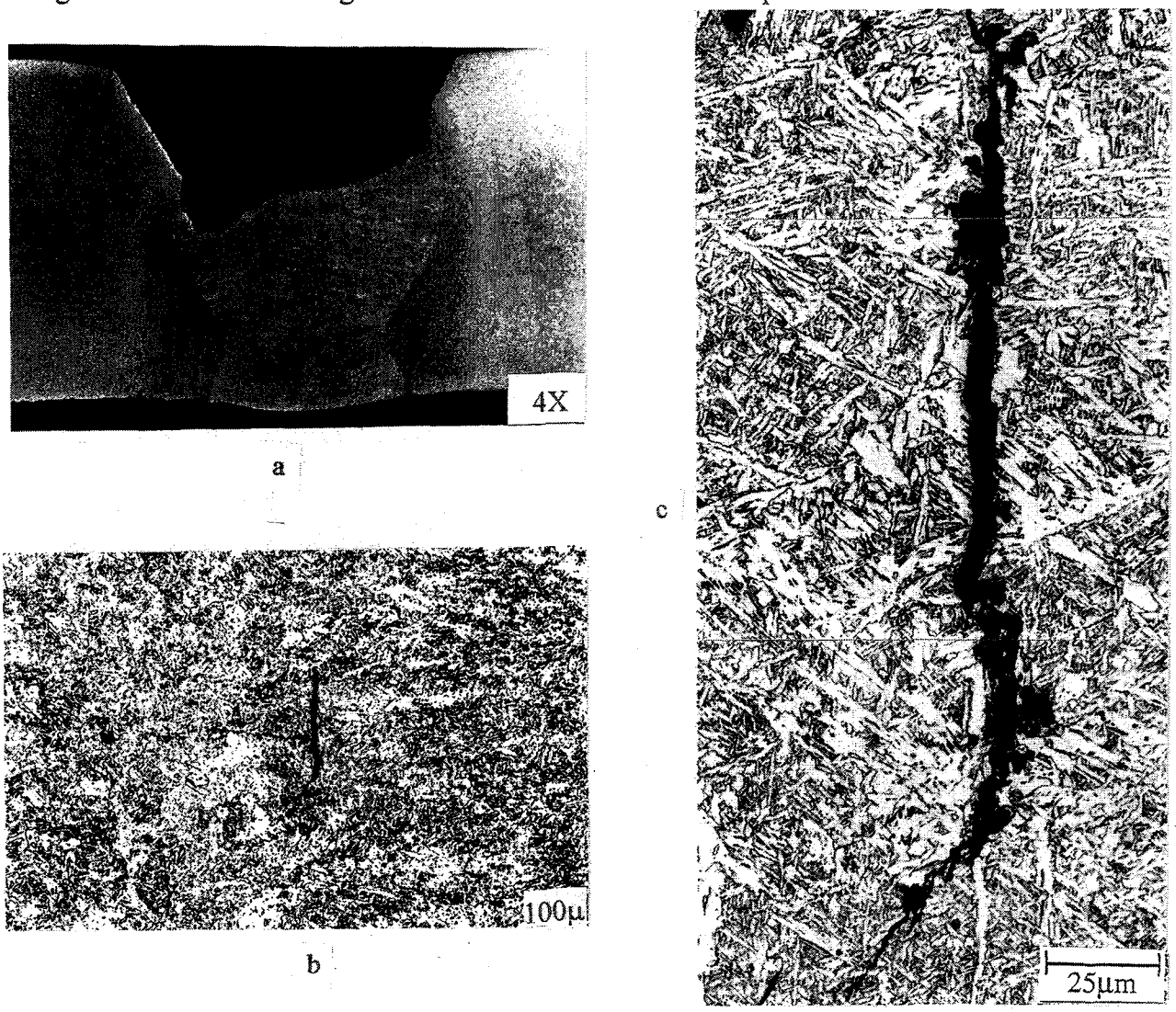

Figure 5.6.2.1 : ***(a) Macrophotograph (b) and (c) Enlarged view of crack at weld centre using E 9010 electrode C.***

Although the position of the crack suggests an origin as solidification crack, only a small segment may consist of a solidification crack, (see figure 5.6.2.2) with extension occurring at lower temperature by HACC.

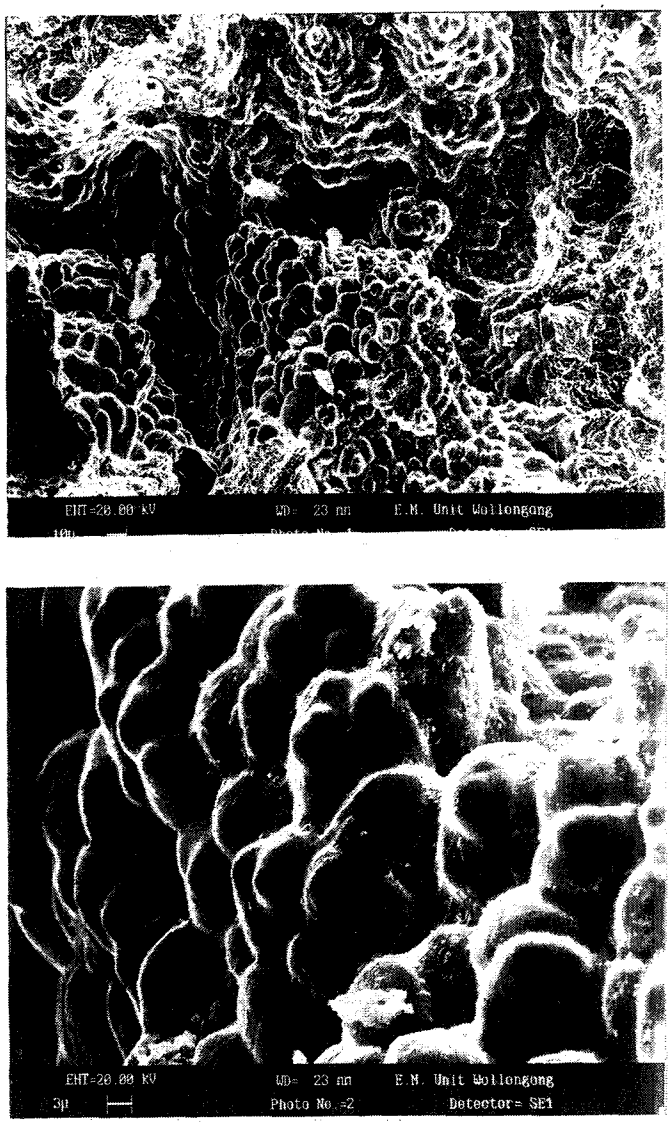

Figure 5.6.2.2.: ***Fractographs of regions showing characteristics of hot cracking***

Chapter Six

6.0 DISCUSSION

Cold cracking in weld metal is believed to be caused by the combination of three factors,

(a) presence of hydrogen

(b) susceptible microstructure and

(c) stress concentration.

It is generally believed that these three factors must be present simultaneously for HACC to occur. This investigation clarifies the effect of preheat temperature on cracking behaviour using cellulosic electrodes on 8.6mm thick X80 pipeline steel. Manual welding was used and localised variations in welding speed which invariably occur, produced uneven bead shape and undercuts which were found to be the critical aspects of cracking in weld metal. Nevertherless, manual welding as conducted in the field and laboratory tests using manual metal arc welding is more relevant to current field welding practices.

Figure 6.1 illustrates the onset of cracking detected from a clip gauge. The initial drop (A) corresponds to the weld contraction during cooling, and the subsequent rise (B) is due to crack initiation in the weld. The second rise in the curve (C) indicates the second stage of cracking. It is evident from the figure that cracking occurred about 6 - 7 minutes after welding.

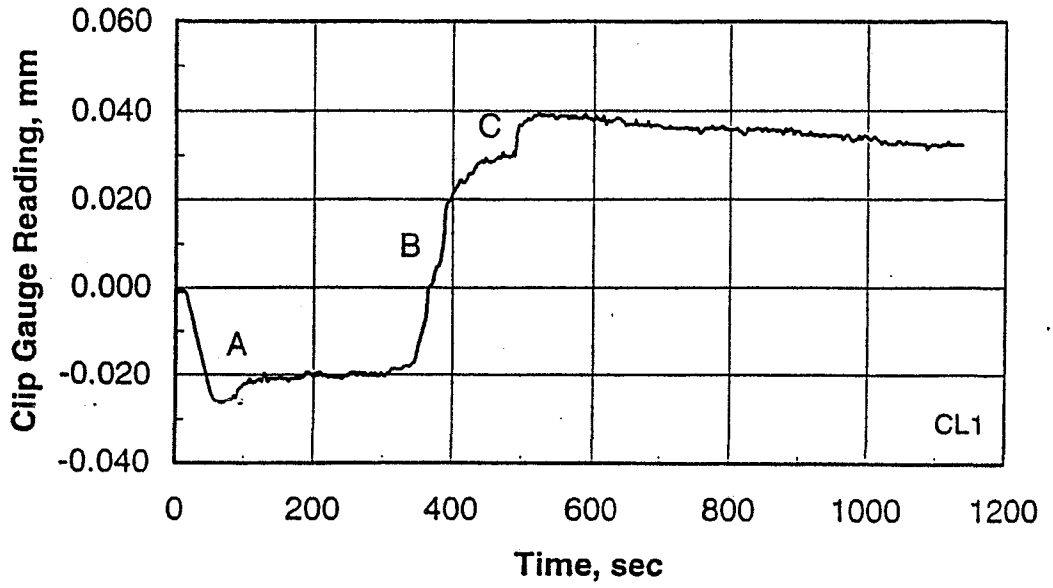

Figure 6.1 : ***Onset of cracking as detected from clip gauge. A: Initial contraction; B: Onset of cracking; C: Second stage cracking [12].***

6.1 EFFECT OF PREHEAT

The WIC restraint cracking test performed with E 9010 electrodes at a preheat of 40°C showed no cracking even for poor weld bead profiles. The lack of cracking in preheated plates is evidently due to increased hydrogen diffusion from the weld metal even at low heat inputs (0.45 kJ / mm). The cooling rate, particularly below 500°C, is strongly influenced by preheat temperature. Dilatometric investigations confirmed that a change in $\Delta t_{8/5}$ with preheat temperature was relatively small (4 to 8 seconds) and not likely to affect significantly the transformation products produced by decomposition of austenite on cooling [13]. Relatively slow cooling rates below 500

C allow more hydrogen to diffuse out of the weld. Below 500°C transformation of austenite is expected to be essentially complete and diffusive loss of hydrogen is likely to be the critical event.

Weld metal deposited from E 6010 showed cracking at room temperature, but no cracking with preheat of 30 °C or more. Although the cooling time for E 6010 weld metal showed no significant change, it can be assumed that the contribution of preheat to microstructural evolution and hence to the effect of microstructure on cracking will be small. Figures 6.1.1. and 6.1.2 show weld metal microstructures produced from E 9010 and E 6010 consumables at two different preheat temperatures. For the E 6010 case the acicular ferrite/bainitic ferrite structure appeared to be finer without preheat but there was little difference in the product phases.

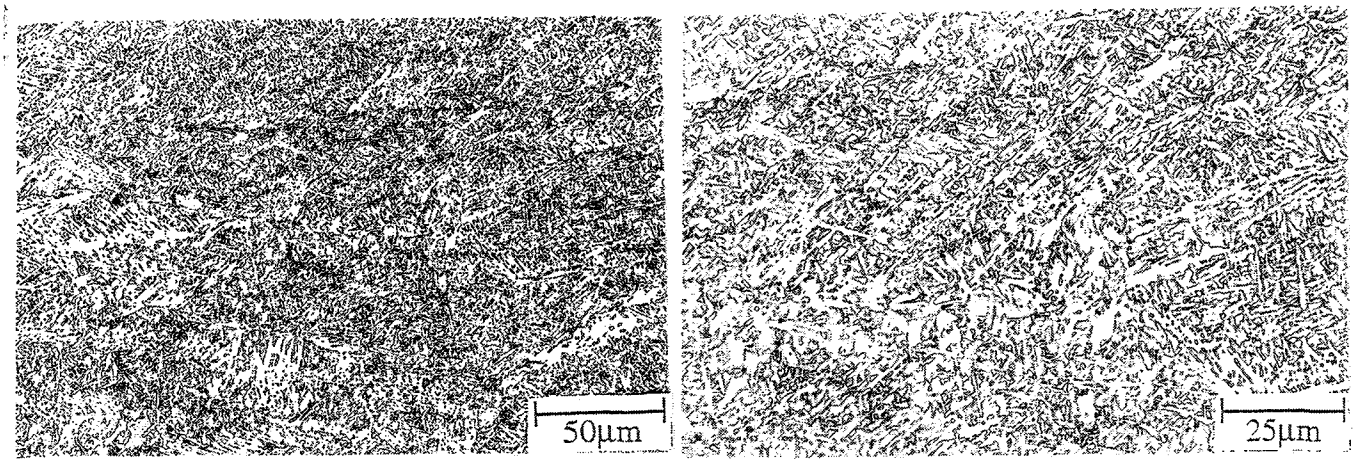

[a]

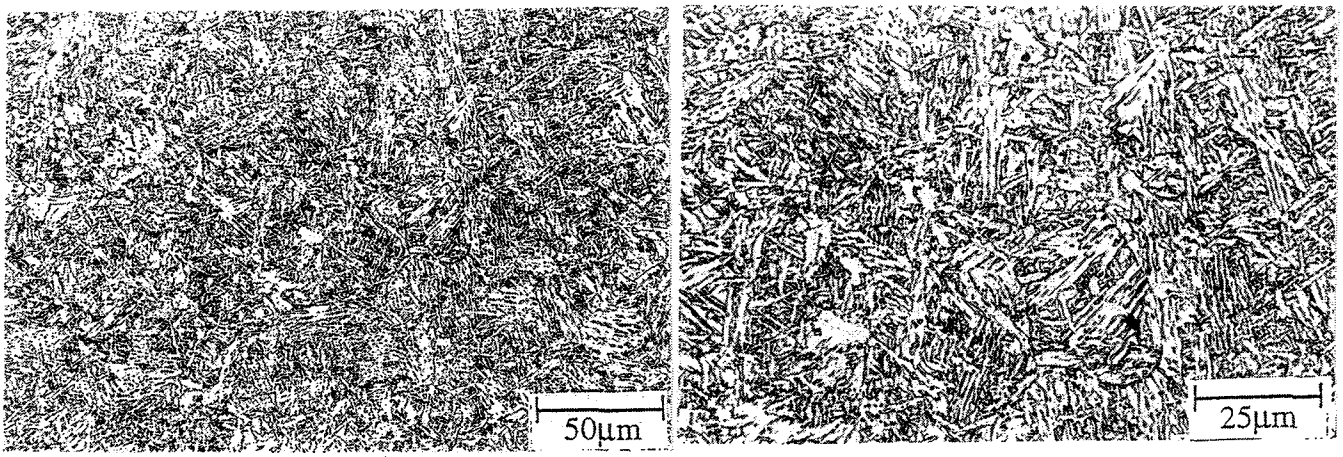

[b]

Figure 6.1.1. : ***Weld metal microstructure from E 6010 electrode C_1 at (a) 22°C and (b) 30°C.***

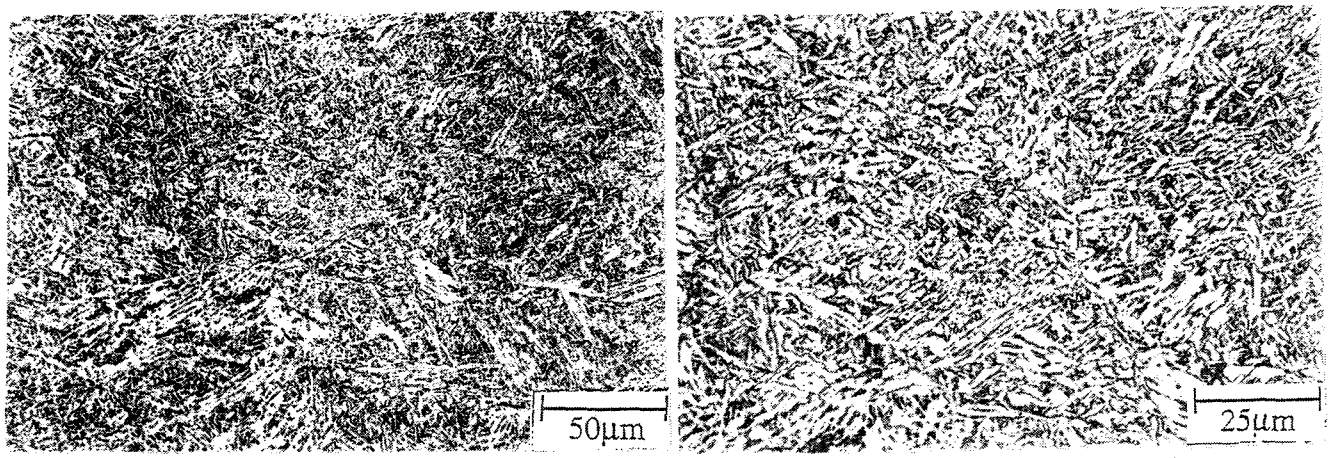

[a]

[b]

Figure 6.1.2 : ***Weld metal microstructure from E 9010 electrode A, (a) 22°C and (b) 40°C.***

The microstructural evolution for the two different preheat temperatures did not show a marked difference due to the small change in $\Delta t_{8/5}$.

6.2 EFFECT OF HYDROGEN

Hydrogen is reported to accumulate at stress concentrator such as the root of the weld some time after welding, when the temperature falls below 200°C. A critical concentration of hydrogen at a stress concentrated region can initiate cracking. By preheating the plates, the critical concentration of hydrogen may not be reached and so cracking is prevented. Earlier results obtained for cooling time [12] show $\Delta t_{8/1}$ for room temperature tests were lower than for preheated test blocks. Cracking was observed in the weld metal for those tests mainly because of weld defects such as undercuts or lack of penetration. However, even at the maximum restraint intensity generated by the standard restraint length of 25mm and the superimposed effect of stress concentrators, no cracking was observed with preheated plates. This observation suggests that hydrogen has a major influence on crack initiation. [13].

6.3 EFFECT OF MICROSTRUCTURES ON CRACKING

Microstructures of the weld metals produced from E 9010 and E 6010 electrodes are shown in the previous chapter (Figures 6.1.1 and 6.1.2). About 50% dilution with the X80 base plate occurred bringing the weld metal composition closer to the base plate composition. The microstructures were typically columnar with the grains growing

from the coarse grained HAZ. Each columnar grain was decorated with proeutectoid ferrite and the grain interior with acicular ferrite and varying amounts of ferrite side plates.

In most of the sections analysed, crack initiation sites were found to be near the weld metal undercut located on the weld surface near the fusion boundary. Microstructurally there was no obvious difference between the center of the weld and the area near the fusion boundary. A significant portion of the crack growth was perpendicular to the columnar grains producing a stepped or staircase configuration. The transgranular segment of the crack passed through acicular ferrite in the grain interior. The acicular ferrite could not resist crack growth due to the stress raising effect of the crack tip and hydrogen accumulation at the top. Cracking was sometimes found to propagate through the HAZ as shown in Figure 6.3.1. The ferrite veins extending from the fusion boundary lie at an angle of about 45° to the direction of the tensile force resulting from restraint due to weld metal solidification. Cracking along the intergranular boundaries can allow progression towards the fusion boundary and then into the HAZ as in Figure 6.3.1. If the columnar grains and the ferrite veins are oriented parallel to the direction of tensile force, the propagation of the crack towards the HAZ will be more difficult as shown in Figure 6.3.2, and the crack will be largely confined to the weld metal.

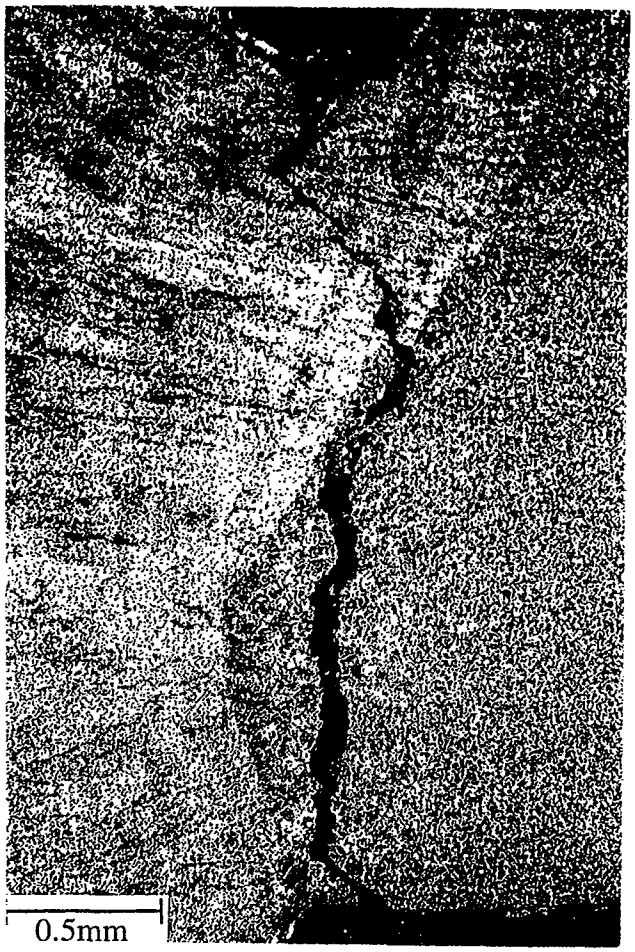

Figure 6.3.1 : ***Crack growth through HAZ. Weld metal deposited using electrode B_1.***

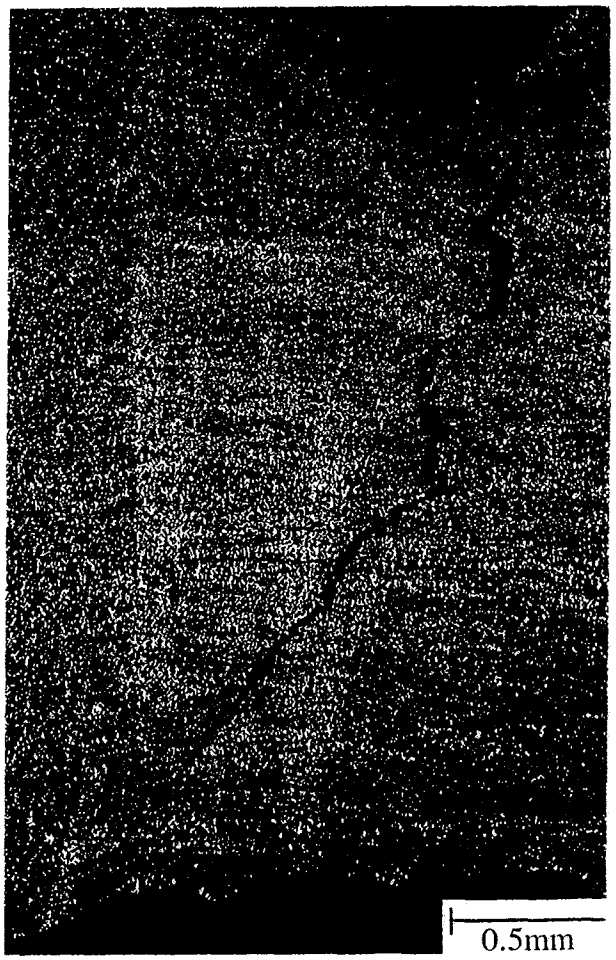

Figure 6.3.2 : ***Crack growth in the weld metal deposited using electrode C.***

6.4 EFFECT OF WELD BEAD SHAPE ON CRACKING

Poor weld shape can play a major role in the crack initiation stage. Once the crack is initiated, the microstructure, tensile forces, stress concentrators and local hydrogen content aid in the extension of the crack. The samples examined, showed a wide variation in weld bead shape. The uneven bead shape indicates deposition rate was not uniform along the length of the weld because of non constant welding speed. Non

uniform speed also resulted in lack of penetration, small throat thickness and undercuts which are principal stress raisers in the initiation of cracking. Figure 6.4.1. shows macrograph of sections with uneven throat thickness and irregular bead shape. The bead shape appeared to be critical to the initiation of cracking. A small irregular throat thickness of the weld resulted in a high local tensile restraint stress during cooling.

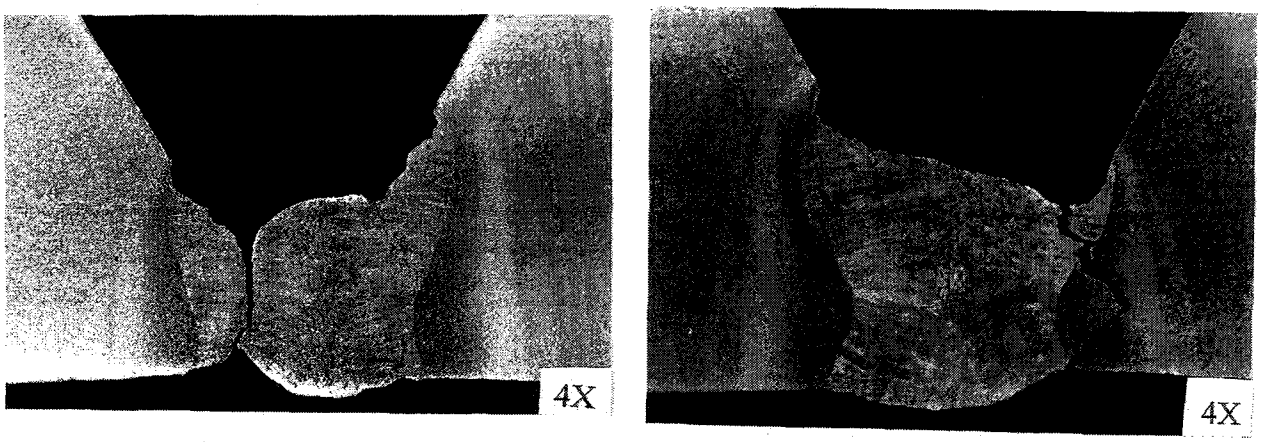

[a] [b]

Figure 6.4.1. : ***Macrophotographs of weld metal showing uneven bead shape. [a] Electrode A and [b] Electrode B_1.***

6.5 EFFECT OF CE AND HARDNESS

The CE values (0.36 - 0.43) for E 9010 and (0.34 - 0.41) for E 6010 electrodes covered relatively narrow bands. Electrode A showed the highest CE value, electrode B had an intermediate value and electrode C showed the lowest CE value of the

E 9010 consumables. The Figure 6.5.1 shows the percentage of cracking calculated for all three electrodes at different preheat temperatures. Although 100% cracking was observed at room temperature, variation in CE values did not significantly influence cracking. Although differences in hardness values from the four different brands of E 9010 electrode deposited (Table 5.6) showed some correlation with cracking propensity, the relative insensitivity of hardness and CE values to cracking is believed to be due to overriding effects of high restraint intensity and fast cooling rates experienced by all of the welds.

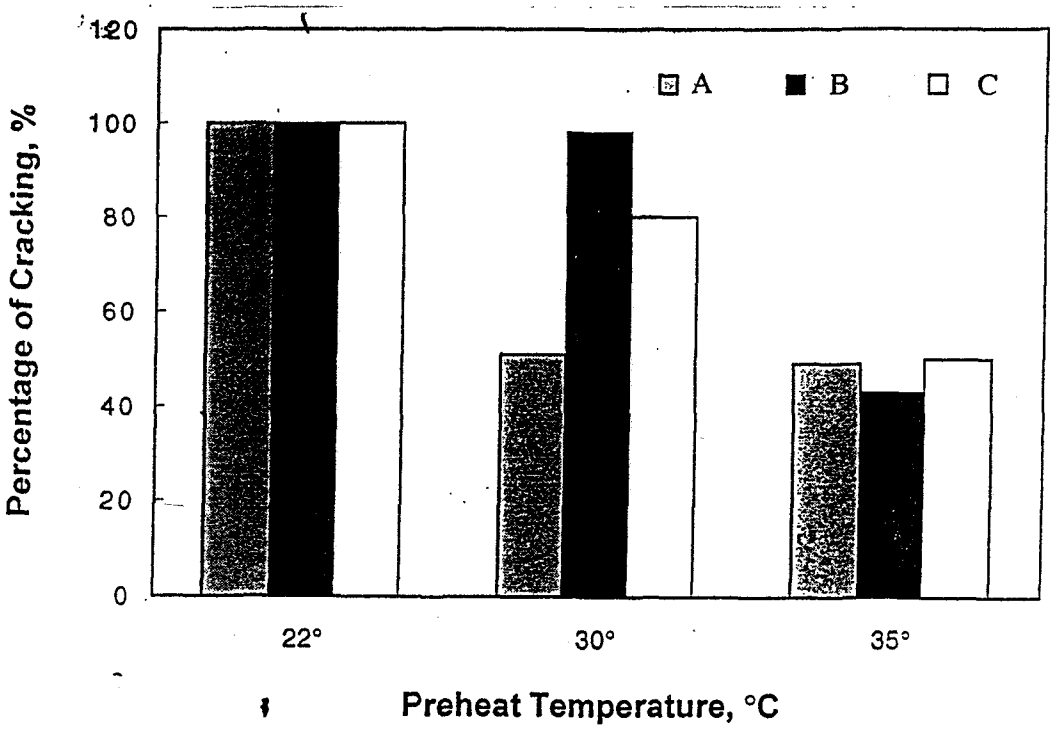

Figure 6.5.1. : ***Cracking percentage for E 9010 electrodes.***

The effect of electrode strength on cracking was established with an undermatching electrode, E 6010. The differences in hardness values did not correlate well with the CE values of the electrodes investigated (Table 5.6). Figure 6.5.2. shows the

percentage of cracking for E 6010 electrodes at room temperature. Hence, it could be concluded that hardness values and CE values cannot be used as tools to predict weld metal cracking in this case. Heat input also was not found to have any major effect on cracking propensity, but the range was only small. Microstructure was also not found to vary significantly with the change in $\Delta t_{8/5}$ (4 - 8 sec) over the narrow range of heat inputs (0.65 - 0.70 kJ / mm). $\Delta t_{8/1}$ for these heat inputs ranges was not found to vary significantly (55 - 60 sec).

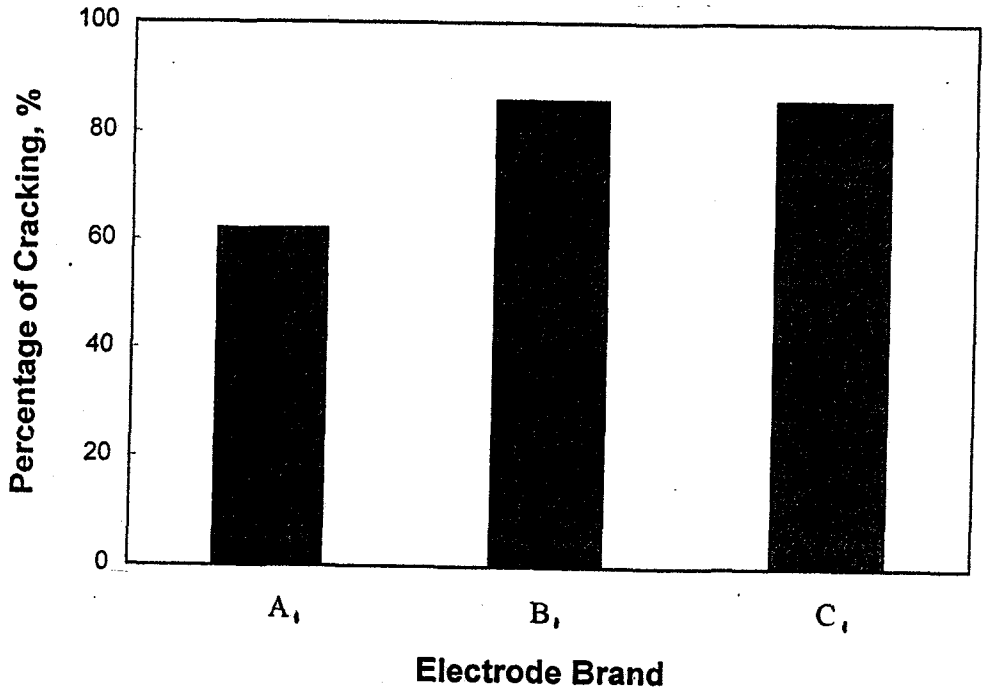

Figure 6.5.2 : ***Cracking percentage for E 6010 electrode at room temperature.***

Electrode	A_1	B_1	C_1
CE	0.34	0.41	0.34
Heat Input kJ/ mm	0.70	0.65	0.65

Table 6.5.2 : ***CE and Heat input for E6010 electrodes at room temperature.***

6.6 CRACKING AND FRACTURE

An attempt was made to characterise the fracture morphologies of HACC and solidification / hot cracking.

6.6.1. Hydrogen Assisted Cold Cracking

A macrophotograph showing HACC is given in figure 6.6.1.1 An enlarged view of the crack is shown in figure 6.6.1.2. Some areas along the fracture path were highlighted and corresponding fracture topography was examined. The examination revealed the fracture mode was a mixture of quasi-cleavage (QC), intergranular (IG) and microvoid coalescence (MVC). The fracture mode in acicular ferrite was ductile associated with fine microvoid coalescence. Figure 6.6.1.3 shows the microstructure and corresponding fracture topography.

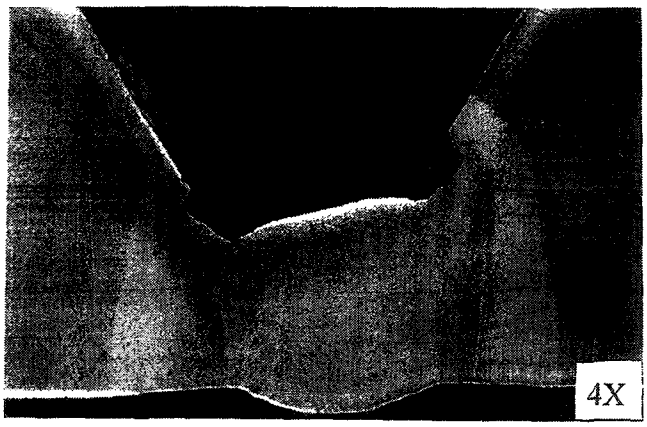

Figure 6.6.1.1.: ***Macrophotograph of HACC in the weld metal deposited using electrode B_1.***

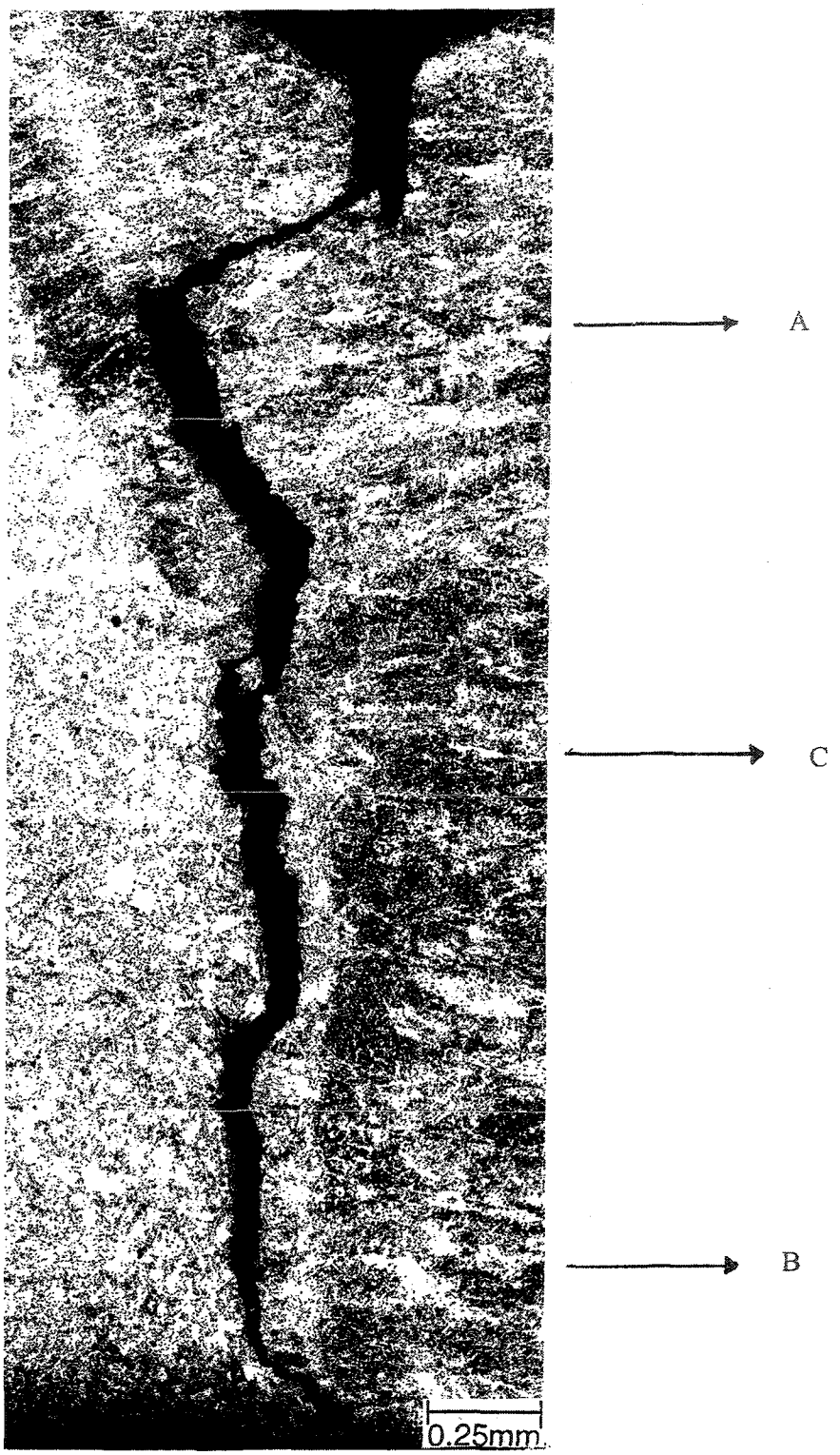

Figure 6.6.1.2 : ***Analysis of crack propagation. (A) Enlarged view of the macrophotograph.***

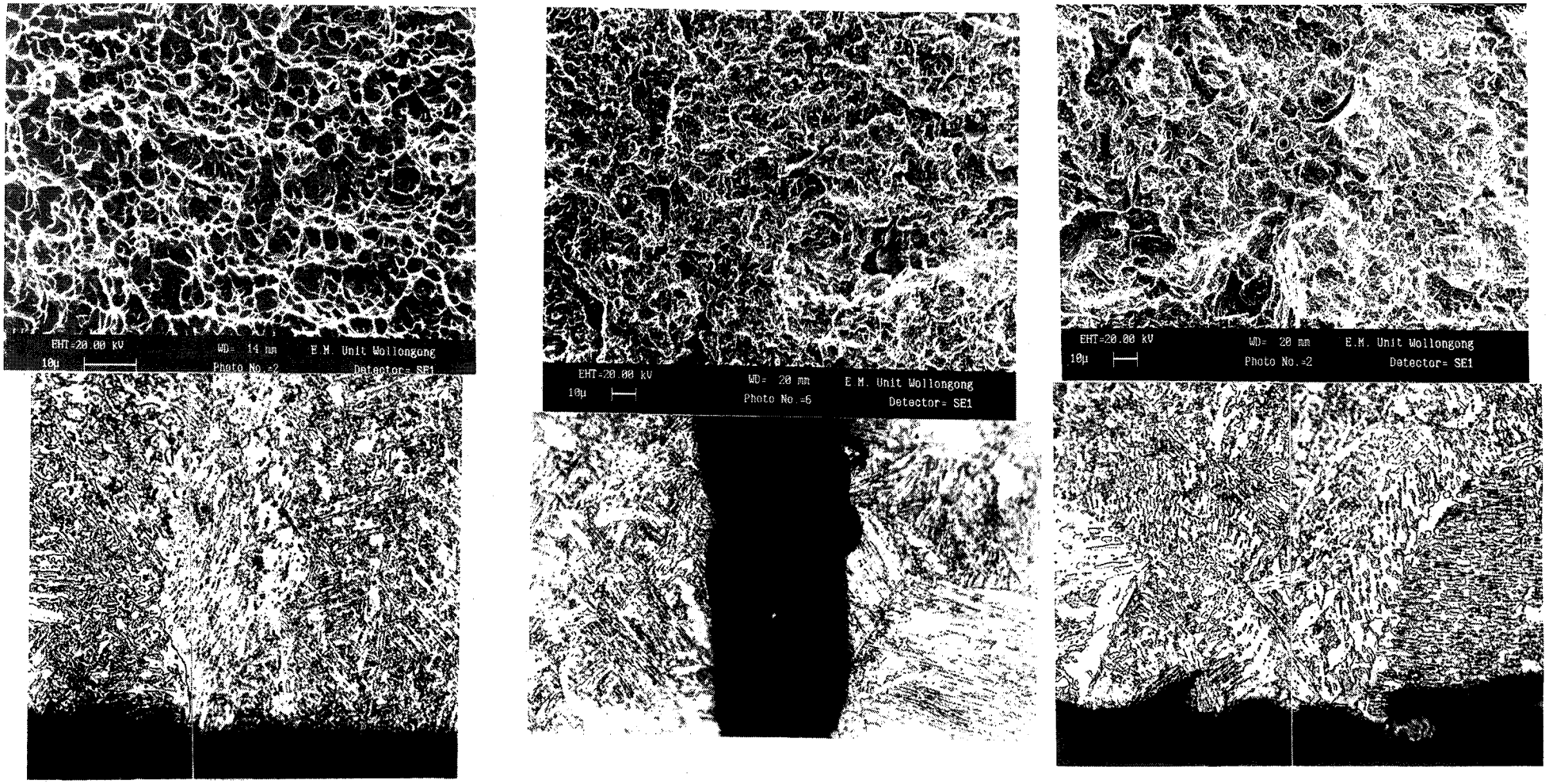

a b c

Figure 6.6.1.3 : The analysis of crack propagation and corresponding fracture topography. (a) Microstructure of weld metal and fracture topography indicated by A in Figure 6.6.1.2. (b) Microstructure of HAZ and fracture topography (quasi-cleavage) indicated by B in Figure 6.6.1.2. (c) Microstructure of HAZ and corresponding fracture topography (quasi-cleavage) of position indicated by C in Figure 6.6.1.2

6.6.2 HOT CRACKING OR SOLIDIFICATION CRACKING

Hot or solidification cracking is believed to be caused by the presence of impurity elements segregated ahead of growing cellular dendritic grains during solidification. However, with the development of modern steels and consumables the influence of impurities on hot cracking has been minimised to a great extent. Many low carbon steels still show ductility troughs over particular elevated temperature ranges and hot cracking in weld metal still remains an issue in pipeline girth welds. It is important to clarify the mechanism and conditions under which it can occur. The correlation between microstructure and fracture topography was investigated and an example is given in figures 6.6.2.1. and 6.6.2.2.

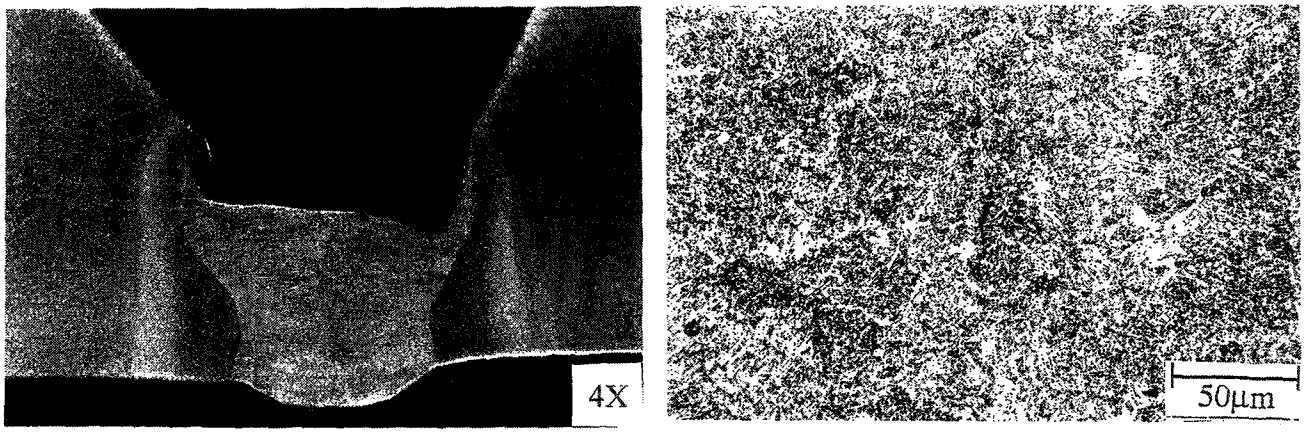

[a] [b]

Figure 6.6.2.1 : ***Analysis of hot crack propagation in the weld deposited with electrode A. (a) Macrophotograph and (b) Enlarged view of the crack.***

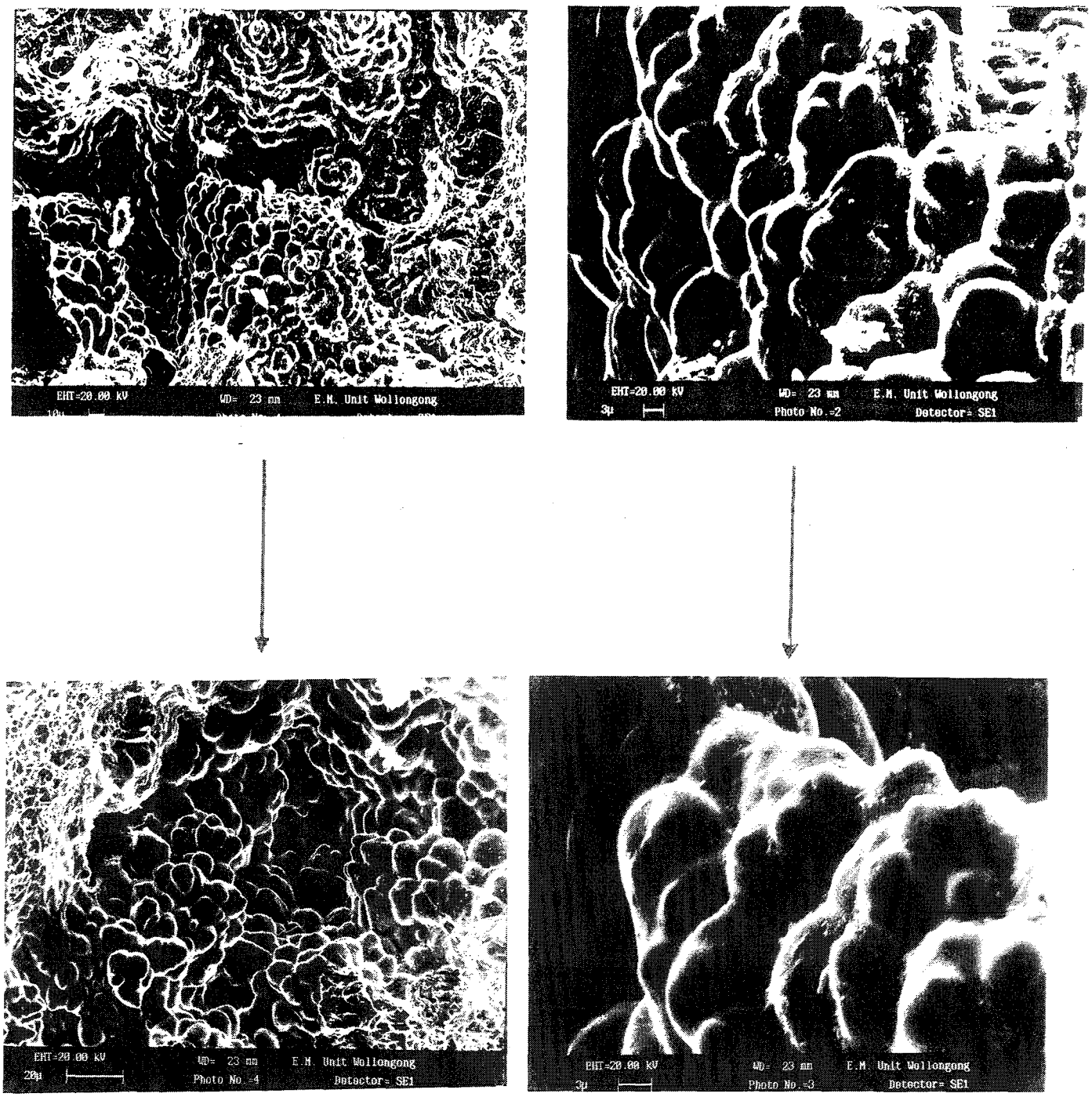

Figure 6.6.2.2 : ***Fractographs of regions showing characteristics of solidification cracking.***

As discussed previously, not all of the central crack showed signs of solidification cracking and after cracking open the sample the pre-existing crack was surveyed to find regions of solidification cracking (Figure 6.6.2.1). It is inferred that solidification occurs in isolated regions near the weld centreline and subsequent extension occurs by HACC at lower temperature. These central cracks create concentrations which promote link-ups with cracks independently nucleated near the undercuts.

CONCLUSION

The analysis of the suitability of E 9010 and E 6010 cellulosic electrodes for root pass welding of X 80 pipeline steel using the WIC restraint cracking test led to the following conclusions.

(1). Most of the tests carried out at room temperature and at the standard restraint length of 25mm with E 9010 and E 6010 cellulosic consumables exhibited cracking in the weld metal.

(2). Preheating to 40°C or more was found to be effective in avoiding cracking in the weld metal deposited with E 9010 electrodes even for defective welds, in which the local stress concentration could be very high.

(3). Preheat of 30°C or more was found to be effective in reducing cracking in the welds deposited with E 6010 cellulosic consumable.

(4). Preheat is effective in controlling cooling rates below 500°C. $\Delta t_{8/1}$ was found to vary much more strongly with preheat than $\Delta t_{8/5}$. This observation is consistent with the hypothesis that cooling rate below 500°C is important in terms of hydrogen effusion from the weld metal.

(5). Variations in cross sectional area of the weld deposit occurred along the length

of the weld due to variations in welding speed. Differences in throat thickness, formation of undercuts on weld metal surface occurred due to poor control of electrode angle. Most of the cracks initiated from or near undercuts.

(6). It was found that cracking in the weld metal occurred within 5 - 10 minutes after welding. When the temperature had fallen below 100°C.

(7). For the range of weld metal compositions, heat inputs and preheats studied, CE and hardness values were not sensitive predictors of HACC in the weld metal.

(8). Columnar grains were found to grow from the fusion boundary roughly at an angle of 45° to the direction of the tensile force and segments of intergranular cracking were commonly observed.

(9). Crack growth also occurred in a transgranular manner across the acicular ferrite, linking up the intergranular segments.

(10). The fracture morphology of HACC was revealed to be a mixture of MVC, quasi cleavage and intergranular fracture.

(11). From the test results obtained with different grades and brands of E 9010 and E6010 electrodes, it can concluded that in principle it is possible to weld X 80 pipe steel without hydrogen cracking, provided the cooling rate is low enough to allow hydrogen effusion to concentrations lower than the critical concentration for crack

initiation.

REFERENCES

(1) Williams. J and Kilmore .C, '*High Strength ERW pipeline steels with improved weldability*', WTIA / APIA Research Panel 7, Joint Research Seminar, Wollongong, Australia, 1995.

(2) Barbaro. F, Williams. J, Meta. A, and Fletcher. L, *'Weldability of X80 linepipe'*, WTIA / APIA Research Panel 7, Joint Research Seminar, Wollongong, Australia, 1995.

(3) Li. H, Alam. N, Chen. L and Dunne. D, '*Hydrogen cracking in high strength thin walled pipeline girth welds'*, WTIA / APIA Research Panel 7, Joint Research Seminar, Wollongong, Australia, 1995.

(4) Fairhurst. W, Booussel. A.J. and Laupresht. W.E., *'Weldability of low carbon Mo - Nb and Mn - Mo - Nb X70 pipeline steel'*, 2nd International conference, London, November, 1979.

(5) ASM Hand Book, *'Welding, Brazing and Soldering'*, ASM International, Materials Park, Ohio, 1991.

(6) Easterling. K, *'Introduction to Physical Metallurgy of Welding'*, 2nd Edition, Butterworth Heinmann, Boston, 1992

(7) Lancaster. J.F, *'Metallurgy of Welding'*, 3rd Edition, London, 1980.

(8) Norrish. J., *'Advanced Welding Processes'*, Institute of Physics, Philadelphia, 1992.

(9) Yeomans. S, *'Welding in Structural steel and Aluminium alloys'*, Department of Civil Engineering, Sydney, April, 1994.

(10) Dunne. D and Alam. N, *'Structures and Property Analysis of E9010 cellulosic electrodes'*, pp38, WTIA, 45th Annual Conference Proceedings, Melbourne, November, 1997.

(11) Perteneder. E, Konigshofer. H and Mlekusch. J, *'The metallurgy and intergrity of high strength MMA girth welds'*, WTIA / APIA Research Panel 7, Joint research seminar, Wollongong, 1995.

(12) Vuik. J, *'An update of the state of the art of weld metal hydrogen cracking'*, Welding in World, vol 31, No 5, 1993.

(13) Alam. N, Dunne. D and Barbaro. F, *'Weld metal crack testing for high strength cellulosic electrodes'*, pp 36, WTIA, 45th Annual Conference Proceedings, Melbourne, November, 1997.

(14) Alam. N, Dunne. D, Squires. I, Barbaro. F and Feng. B, *'Weldment cold cracking - The effect of hydrogen and other factors'*,

(15) Graville. B, *'A survey review of weld metal hydrogen cracking'*, Welding in the World, Vol 24, No 9/10, pp 190 - 198, 1986.

(16) McParlan. M and Graville. B.A., *'Hydrogen cracking in weld metals'*, Welding Research Supplement, American Welding Journal, AWS, 1987.

(17) Beachem. E.P, Johnson. H.H and Stout. D.R, *'Hydrogen and Delayed Cracking in Steel Weldments'* Welding Research Supplement, American Welding Journal, AWS, Oct, 1991

(18) Harasawa. H, Ikoma. T and Nmioka. T, *'Prevention of cold cracking in pipeline girth welding by use of high -cellulose electrodes'*, Third International Conference in Pipe Welding, London, November, 1986.

(19) Huika. K, Heisterkamp. F and Bersch. B, *'Weldability of newly developed X75 and X80 for large diameter pipelines'*, third international conference, London, 1986.

(20) Sawhill. M.J, Baker. J.C and Howe. P, *'Hydrogen assisted cracking in high strength pipeline steels'*, Welding research supplement, American welding Journal, AWS, July, 1986.

(21) Signes. G.E and Howe. P, *'Hydrogen assisted cracking in High strength pipeline steels'*, Welding research supplement, American welding Journal, August, 1988.

(22) Evans. G. M, *'Microstructural and Properties of ferrite steel welds containing Al and Ti'*, Welding research supplement, American welding journal, AWS, August 1995.

(23) Phelps. B, *'Weldability testing of linepipe steels using cellulosic manual metal arc electrodes'*, Doc XI - E, P7 - 13, May 1977.

(24) Smith. N. J, McGrath. J. T, Giannetto. J. A, and Orr. R. F, *'Microstructure / Mechanical properties relationship of Shielded metal arc welds in HSLA 80 steel'*, 16th annual AWS meeting, New Orleans, April, 1988.

(25) Bracarense. A. Q and Liu. S, *'Chemical composition variation in shielded metal arc welds'*, welding research supplement, American welding journal, AWS, December, 1993.

(26) Mota. J. M. F and Apps. R. L, *'Chevron cracking' - A new form of hydrogen cracking in steel weld metals*, welding research supplement, American welding journal, AWS, July, 1982.

(27) Avner. S. H, *'Introduction to Physical Metallurgy'*, Second edition, Materials Science and Metallurgy series, 1994.

(28) Baker. R. G and Watkinson. F, *'The effect of hydrogen on the welding of low alloy steel'*, British Welding Research Association, Abington Hall, 1974

(29) Chakravarthi. A. P and Bala. S. R., *'Evaluation of weld metal cold cracking using G BOP test'*, Welding Research Supplement, American Welding Journal, AWS, January, 1989.

(30) Alcantara. N. G and Rogerson. J. H, *'A prediction diagram for preventing hydrogen assisted cracking in weld metal'*, Welding Research Supplement, American Welding Journal, AWS, April, 1984.